ROMA TRE
UNIVERSITÀ DEGLI STUDI

DOCTORATE IN APPLIED ELECTRONICS

XXIX CYCLE

HUMAN BODY ENERGY HARVESTING FOR ACTIVITIES RECOGNITION

PhD student: Antonino Proto

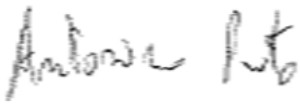

Tutor: Maurizio Schmid

PhD coordinator: Enrico Silva

Table of contents

SUMMARY **3**

1 INTRODUCTION (A) **4**

1.1 MOTIVATION 4

1.2 ENERGY HARVESTING PERSPECTIVE 5

2 LITERATURE REVIEW (B) **9**

2.1 BIOMECHANICAL ENERGY HARVESTING BY PIEZOELECTRIC TRANSDUCER 10

2.2 HUMAN HEAT ENERGY HARVESTING BY THERMOELECTRIC GENERATOR 13

2.3 NANOGENERATORS FOR HUMAN BODY ENERGY HARVESTING 15

2.3.1 PIEZOELECTRIC NANOGENERATORS 16

2.3.2 TRIBOELECTRIC NANOGENERATORS 18

2.3.3 THERMOELECTRIC NANOGENERATORS 21

2.3.4 FABRIC NANOGENERATORS 22

2.4 TEXTILE SENSORS FOR BIOMECHANICAL SENSING 24

3 ENERGY HARVESTING FROM HUMAN HEAT (C) **27**

3.1 HUMAN BODY THERMAL CHARACTERISTICS AND ENVIRONMENTAL ASPECTS 27

3.2 TECHNIQUES FOR HARVESTING THE HUMAN HEAT ENERGY 31

3.3 EXPERIMENTAL SECTION 34

3.3.1 THERMOELECTRIC GENERATOR CHOSEN 34

3.3.2 TEG PLACEMENT ON HUMAN BODY and PERFORMED ACTIVITIES 35

3.3.3 A FABRIC BAND TO SUPPORT THE TEG 35

3.3.4 EXPERIMENTS AND DATA DISCUSSION 37

4 HUMAN BODY MOTION: ENERGY HARVESTING AND DETECTION OF GAIT PHASES (D) **47**

4.1 BIOMECHANICAL CHARACTERISTICS OF THE HUMAN GAIT 47

4.2 TECHNIQUES FOR HARVESTING THE BIOMECHANICAL MOTION 51

4.3 EXPERIMENTAL SECTION 54

4.3.1 PIEZOELECTRIC TRANSDUCERS CHOSEN 54

4.3.2 HUMAN BODY MOVEMENTS CHOSEN 56

4.3.3 CHOICE on DAILY ACTIVITES 56

4.3.4 INTEGRATION INTO A SUIT: ELASTIC COTTON FABRICS 57

4.3.5 HUMAN BODY ENERGY HARVESTING – EXPERIMENTS AND DATA DISCUSSION 59

4.3.6 DETECTION OF GAIT PHASES – EXPERIMENTS AND DATA DISCUSSION 69

5 GENERAL CONCLUSIONS (E) **74**

LIST OF FIGURES **80**

LIST OF TABLES **82**

REFERENCES **83**

KEYWORDS **92**

SUMMARY

Nowadays, the research field of the energy harvesting from the human body is attracting great interest in the scientific community, with the objective of designing new ways of capturing energy sources to power wearable devices. Smart wearable devices are increasingly being used in different health-related application fields, thanks to the low cost and to the availability of miniaturized technology, and this makes it possible to capture variables associated with the health and safety status of the human being. Unfortunately, the battery size of these devices determines their operating time, thus limiting applicability for the long-term monitoring. Among all the technologies for harvesting the energy from the environmental sources, this PhD thesis deals with recovering the energy directly from devices placed onto the human body surface. In particular, the motion of the limbs during the daily physical activities and the continuously wasted heat are the recoverable energies that were specifically targeted in this PhD thesis. Therefore, the proposed thesis reviews both flexible technologies for biomechanical energy harvesting and miniaturized devices for recovering the thermal energy on the body surface, with a specific focus on those technologies able to minimize discomfort to the wearer. In the experimental sections, two commercial technologies, one piezoelectric and one based on the Seebeck effect, were tested for understanding the real possibility of harvesting the biomechanical and thermal energies, respectively. For both technologies, the range of the values of the power output is about 1 – 10 μW, by employing just a harvester for each test. In addition, measurements performed to evaluate the ability of such devices to the main phases of the gait cycle were made by using the piezoelectric transducer on the back side of the knee joint. The results show the feasibility to detect the phases of gait cycle by using a passive device. Therefore, these tests may help contribute to the route of innovation for developing self-powered monitoring systems.

INTRODUCTION (A)

1.1 MOTIVATION

The recent trend for biomedical engineers who are studying the safety and health of human beings is to develop compact and wearable measurement systems for continuously providing information about the vital parameters [1-3]. Wearable sensor nodes are a modern way to monitor the health status of people, as they are practical, comfortable and not invasive [4, 5]; they are low-cost and able to communicate with processing devices, such as PCs, smart-phones or radio stations [6, 7].

Wearable devices play an important role in everyday life, since they are suitable for a wide range of applications. For example in medical science, the wearables gather diagnostic data and monitor the patient's progress in the recovery process [8], or for the elderly they allow the context of telemedicine, through the monitoring of the health status at home [9]. Again, in sports and wellness contexts, wearables can help the users for increasing their training performances and the quality of life, by means the classifying of motor tasks and activities of day-life [10, 11]. In addition, in the context of security, wearables can provide information about the exact location of people, such as the position of firefighters, or army troops engaged in dangerous tasks [12].

Generally, a network of multiple wearable devices lets to capture many bio-parameters on the human body, such as body temperature, ECG, EMG, and EEG among many others. Thus, the set of wearables allow creating a “body sensor network” (BSN) able to communicate the acquired bio-signals with the external world [13, 14]. Unfortunately, one of the main obstacles for a BSN could be the power necessary to keep each wireless sensor node on [15]. The battery size of these sensors determines their operating time, thus limiting applicability for long-term monitoring. A big battery size allows long-time monitoring, but it is not comfortable for users, since the dimensions of the

device do not warrant wearability, and may introduces artifacts associated with the movement of the sensor attached to the body. By using ultra-low-power electronic components could be a way to reduce the power consumption of a BSN, but it does not eliminate the problem of the unlimited monitoring. Therefore, the study of the techniques for harvesting the energy on the human body is imperative for developing a new class of self-powered monitoring devices.

1.2 ENERGY HARVESTING PERSPECTIVE

The energy harvesting from environmental sources is a solution for solving the problem of limited operating time of the devices, since the nature is an invaluable and endless source of energy. Between all the energy sources, the environmental power sources more widely available are the following: light, thermal, electromagnetic radiations and mechanical vibrations. Vullers *et al*. [16] reviewed the characteristics of these energy sources and the corresponding power which can be harvested from them. ***Table 1A*** shows these power values. The researcher pointed out that the power recovered in the environment is in the range: 100 nW – 10 mW, which is a typical power range for supplying energy to wireless sensor nodes. ***Figure 1A*** shows a list of commercial off-the-shelf (COTS) components and devices in order to understand what could be the practical use of the power generated from the energy harvesters. The values of the power consumption for COTS and devices in ***Figure 1A***, were obtained from datasheets for the COTS, and from the paper proposed by Campagnolo and Kroiss [17] for the other devices. In ***Figure 1A***, the integrated circuit components (ICs) are in all the power range values. It means that ICs with high values of power consumption, such as wireless microcontrollers and digital signal processors have incorporated more simple functions, as those shown by ICs placed in the range 100 nW – 10 μW. As regard the generic sensors for electronic circuits, most of them are in the value range 1 μW – 10 μW and the implantable medical devices are in the range around 10 μW – 1mW.

Table 1A. *Characteristics of different energy sources available in the environment, and the corresponding harvested power.*

Source	Source Power	Efficiency	Harvested power
Ambient light			
Indoor	0.1mW/cm^2	5 – 30 %	10 μW/cm^2
Outdoor	100 mW/cm^2		10 mW/cm^2
Vibration / motion			
Human	0.5 m @ 1 Hz , 1 m/s^2 @ 50 Hz	1 – 10 %	4 μW/cm^2
Industrial	1 m @ 5 Hz , 10 m/s^2 @ 1 kHz		100 μW/cm^2
Thermal Energy			
Human	20 mW/cm^2	± 0.1 %	30 μW/cm^2
Industrial	100 mW/cm^2	± 3 %	1 – 10 mW/cm^2
RF			
Cell phone	0.3 μW/cm^2	± 50 %	0.1 μW/cm^2

These data suggest improving the investigation on development of EHs able to produce the power supply needed for designing of sustainable (i.e. self-powered) devices.

In short, energy harvesting systems can be used in three different ways: *as a replacement of the battery in ultra-low power systems*; *to increase the life cycles of devices*; *to recharge batteries*.

Battery replacement in ultra-low power system, where the total power consumption is around 1 mW, is possible, as many integrated circuits on the market consume less than 100 μW (***Figure 1A***). Again, *the energy harvesting system can prolong the operating time* of implantable devices, such as the cochlear implants, the cardiac pacemakers or devices for the neurostimulation [18]. Finally, the last way to use the energy harvesting system is *to recharge batteries*. Sodano *et al*. [19] proposed a comparison between mechanical EHs for recharging batteries: when the amount of the harvested energy is not compatible with the amount of the energy requested by the device, the first can be used as a reservoir for allowing the battery charging.

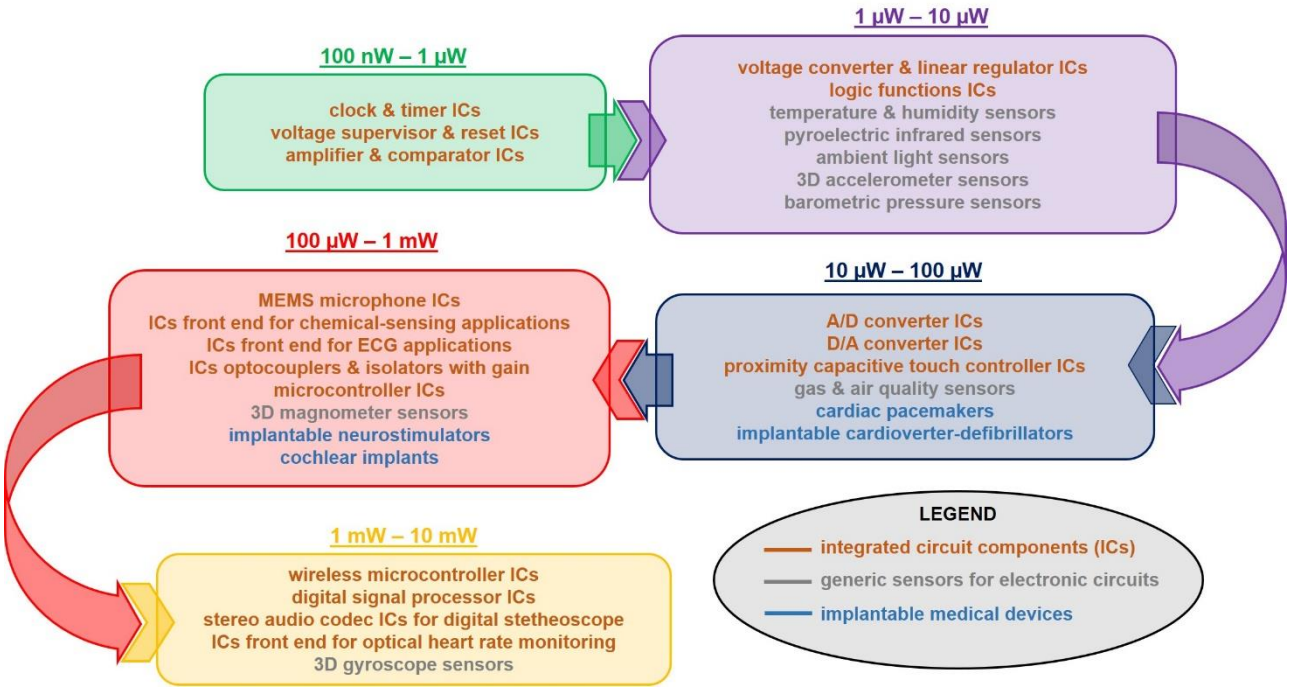

Figure 1A. The average power consumed by generic integrated circuit components and sensors, and by implantable devices, in the range of values: 100 nW – 10 mW. The color codifies the ranges: green: 100 nW - 1 µW, violet: 1 µW - 10 µW, blue: 10 µW - 100 µW, red: 100 µW - 1 mW, yellow: 1 mW - 10 mW.

Overall, this thesis focusses on harvesting the energy on the human body, and it offers information regarding the techniques for recovering the energy directly on the surface of the body.

The proposed PhD thesis proceeds as follows. The chapter 2 discusses the literature review about the biomechanical energy harvesting by piezoelectric transducer and the human heat energy harvesting by employing the thermoelectric generators. Then, the literature review chapter focuses on the newest technology for harvesting the energy from the environment. This technology is represented by the development of the nanogerators. To conclude the chapter 2, the research field of the sensing of physiological parameters by means smart textiles is reviewed, in order to introduce the design aspects related to the integration of the energy harvesters into common fabrics.

The chapters 3 and 4 present and discuss original results of the experimental tests concerning the biomechanical and thermal energy harvesting on human body. In addition, chapter 4 shows the preliminary results about the feasibility study of using a biomechanical energy harvester

for the classification of the main phases of the human gait: the stance and swing phases, respectively.

Finally, chapter 5 introduces the general conclusions and the possible future perspectives for the field of the human body energy harvesting for activities recognition.

LITERATURE REVIEW (B)

Energy harvesting on human body is a research field under rapid development. The energy recovering directly on the body plays an important role to overcome the issue of continuous powering for wearable devices. Since the researcher T. Starner in 1996 hypothesized a wearable computing powered by the energy of human body [20], many researchers improved the techniques for developing energy harvesters on the body surface.

From an energy perspective, the human body is a relevant warehouse of energy: it provides potential power sources, such as the biomechanical energy through the body movements and the thermal energy by the exchanged heat with the environment. In such a way, the power source on human body are those biomechanical and thermal.

As predictable, the working efficiency of an energy harvester placed on the body depends on the time of the day, which determines oscillations in the quantity of energy at hand; considering the variations of physical activity as a function of day time, and the heat variations associated with environmental temperature changes. By dividing the day into four time periods, it is possible to analyze and qualify the energy recovery for each environmental source. ***Figure 1B*** shows the energy maintenance of each singular energy harvester. It represents the ability of the energy harvester, in relation to an established period of the day, to recover energy, and it describes the energy harvester working efficiency depending on the activity performed by human beings and depending on the environmental conditions that surround them. For example, at night, during sleep the major source of energy is the temperature gradient, since the movement of the body is minimal. Concerning the curve trend for thermal harvester, it reaches the lowest point in the morning hours between four and seven, and the highest in the evening between five and eight [21]. Concerning the energy

recovered by body movement, it is minimal during the night, and reaches peaks in correspondence to those hours when on average, motion is involved [22, 23].

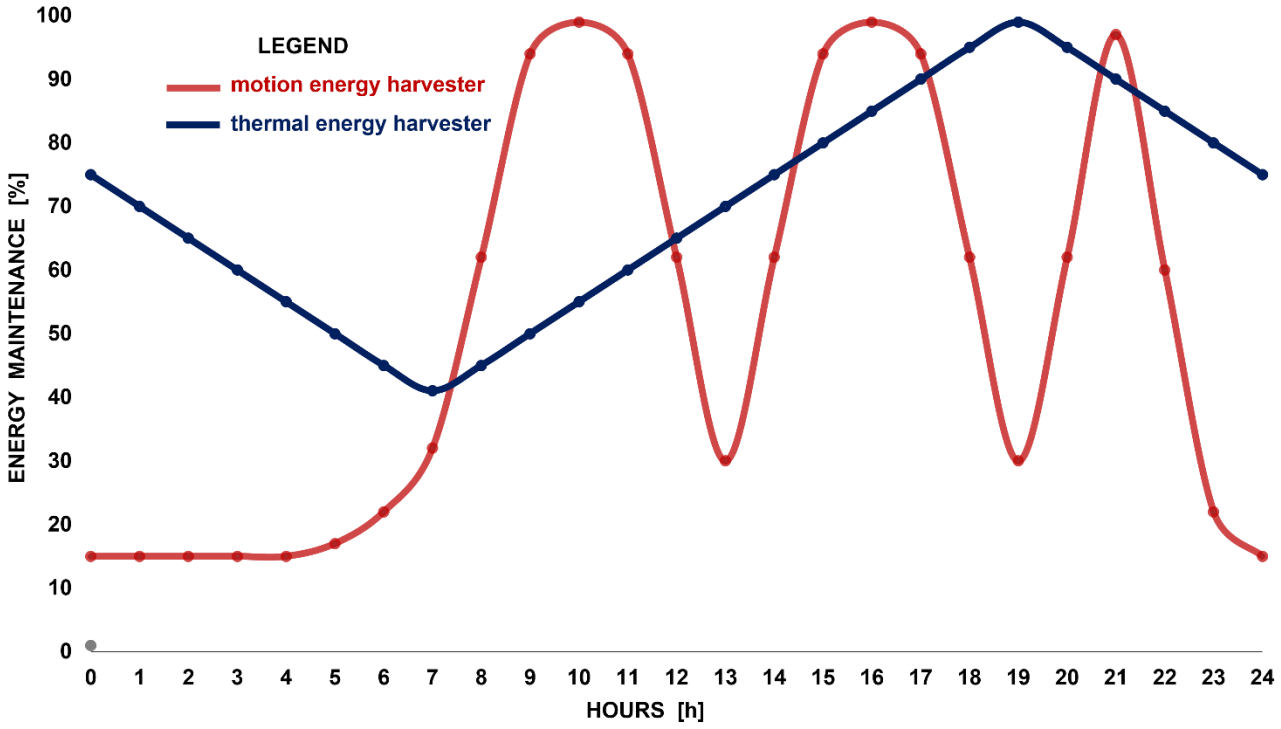

Figure 1B. *The energy maintenance in percentage, during the day. The color codifies the energy harvesters: Red – motion energy harvester, Blue – thermal energy harvesters.*

The main goal, at this point, is to understand the wearability of the harvesters and their efficiency in terms of power output. For this purpose, the next two sections reviewed the biomechanical and thermal energy harvesters for recovering the energy directly on the body. Then, the new technology of nanogenerators for harvesting the energy will be reviewed. Finally, a brief section show the possibility to monitor the health status by using the e-textile technology.

2.1 BIOMECHANICAL ENERGY HARVESTING BY PIEZOELECTRIC TRANSDUCER

The biomechanical energy harvesting is a subcategory of the broader category of energy harvesting from environmental vibrations. While the energy harvesting from environmental vibration has been extensively studied recently [24], the biomechanical energy harvesting is quite a new research field for scientist.

The mechanical energy of the environmental vibrations can be converted into electrical energy by electromagnetic, electrostatic, magnetostrictive and piezoelectric transducers: in the studied literature, the electromagnetic, electrostatic and piezoelectric transducers dominate. The work presented by Roundy [25] provides a general theory that can be used to compare these different transduction approaches. In conventional macro-scale engineering, environmental vibration transducers are mostly based on the electromagnetic technique, while in small-scale energy harvesting, the electrostatic and the piezoelectric transducers are more practical and better suited to the microelectromechanical (MEMS) implementation [24]. The main difference between piezoelectric and electrostatic transducers is that the electrostatic transducer must be powered to operate [26], and therefore the piezoelectric transducers are the best choice for addressing the goal of the proposed thesis.

In the current scientific literature, we denote several examples of piezoelectric energy harvesters. Generally, they are divided based on their placement on the body parts and on the constituting material type [27].

The most common types of materials for the piezoelectric transduction are lead zirconate titanate (PZT) and polyvinylidene fluoride (PVDF). Other piezoelectric materials are the barium titanate ($BaTiO_3$) [28], the micro-fiber composites (MFC) [29], the active fiber composites (AFC) [30], and the piezoelectric fiber composites (PFC) [31]. In addition, new materials, such as the lead magnesium niobate-lead titanate (PMN-PT) [32] and the zinc oxide nanowires (ZnO-NWs) [33] are also materials with interesting piezoelectric physical properties.

When comparing the PZT and PVDF transducers [34], the former ones are better in terms of transduction coefficients, while the latter ones are less expensive and more flexible, and they can add pyroelectric properties. PZT transducers can be divided into two categories: hard PZT and soft

PZT. Hard PZT are generally not suitable for the field of the biomechanical energy harvesting because they are not flexible enough to accommodate the body joint rotations.

As regards to the energy harvester classification about their placement on the body surface, Renaud *et al*. [35] designed a piezoelectric transducer mounted on the human wrist able to theoretically generate up to 40 $\mu W/cm^3$. Again, Jung *et al*. [36] developed a curved piezoelectric generator placed into a watch strap able to produce 3.9 mW/cm^2 of power density from the low frequency, such as the activities related to the locomotion of the body. Instead, regarding the possibility to integrate the piezoelectric harvester into a shoe insole, Shenck and Paradiso [37] published the most relevant work for the current literature: they introduced a system composed by a flexible piezoelectric stave placed under the insole and a hard dimorph piezoelectric element placed into the insole. The system could harvest up to 9.7 mW at 0.9 Hz of walking pace. Concerning the possibility of harvesting the energy through a backpack, Feenstra *et al*. [38] developed a system by replacing the strap buckle with a piezoelectric stack actuator, which generates 0.4 mW from the differential forces between the wearer and the pack. In addition, Shukla and Bell [39] reported a novel concept of harvesting biomechanical energy from the low frequencies and forces of the human gait movement, through a device attached to the waistline; the maximum power output for this system was nearly 300 μW. Finally, for harvesting the biomechanical energy on the legs, Pozzi *et al*. [40] proposed a plucked piezoelectric bimorphs for the knee-joint energy harvesting. The system had the potential to produce a sustained power of several mWs during the walking activity. Again, De Pasquale and Somà [41] used a piezoelectric transducer to find out an output power of 0.33 μW associated to the angular displacement of the knee joint during walking.

Despite a large body of literature focusing on the development and testing of the biomechanical energy harvesting systems, to the author knowledge there is a notable lack of studies

targeting the optimization of harvester kinds, and their placement, to be used in everyday life activities, without feeling discomfort to the wearer.

2.2 HUMAN HEAT ENERGY HARVESTING BY THERMOELECTRIC GENERATOR

Thermoelectric generator (TEG) produces electrical energy by exploiting the thermoelectric effect. The thermoelectric effect implies a voltage generation across two dissimilar semiconductors when a temperature difference occurs between them. The application field of the human heat energy harvesting concerns the recovery of dissipated body heat, by exploiting the thermoelectric effect.

At the end of '90s, the *Seiko Company* developed the first wristwatch powered by a TEG [42]. The proposed TEG consisted of 10 modules, which are connected in series by using gold wires, and the total power output was about 22.5 μW. This amount of power could drive the watch and simultaneously recharge its battery, since the value of the power output was 20 times the amount needed for driving the watch (1 μW). After that, many researchers hardly worked for designing wearable devices powered by the human heat. The IMEC group is one of them. Between 2004 and 2008, they developed several wearable devices, directly powered by the human heat. At first, Leonov *et al*. [43] designed a watchstrap for the study of thermal features of human body, by using a single layer TEG made by 128 thermocouples connected in series. Then, they developed a 4-layer TEG with 5000 thermocouples, for powering a conventional pulse oximeter [44]. The 4-layer TEG generated a power value up to 200 μW when a temperature difference of about 8 °C occurred between the two sides of the generator. This amount of power could supply energy for the wireless transmission of the pulse oximeter acquired data. In addition, in 2008 the same group of research developed a self-powered 2-chaneel electroencephalography system [45]. In this system, the area for the hot side of the TEG was about 64 cm^2, and measured power output reached up to 2.2 mW.

The authors claimed that the forehead is the best position for harvesting the human heat energy, since the forehead provides the largest heat flow on a quite big area. Again, the researchers of the IMEC group proposed in 2009, the first example of shirt for recovering the thermal energy on the body during the performance of normal daily activities [46, 47]. In the shirt, 14 TEG modules with an area size of about 12 cm^2 each, generated up to 1 mW during working activity at office and, in the case of walking, the power value reached up to 2 – 3 mW in a sunny day.

All of these systems for thermal body energy harvesting rely on the positioning of a heatsink on the cold side of the TEG. The heatsink is necessary to improve the thermal coupling with the environment in order to maximize the power produced by the thermoelectric generator [48].

As regards recovering the human heat energy directly on the arm, Lossec *et al*. [49] proposed a system composed by the stacking of two TEGs with a black heatsink on its cold surface. The black surface increase the emissivity of the cold side and the value of its heat transfer/radiation coefficient with the environment. The researchers stated that the values of the power output of the improved system with the black heatsink reached up to 7 $\mu W/cm^2$ in rest conditions and 30 $\mu W/cm^2$ during walking, by a temperature difference of about 15 °C. Again, Voss *et al*. [50] proposed another system for recovering the heat energy on the arm: the researchers placed a Velcro strap with an integrated TEG on the upper arm to produce electrical energy by performing locomotion activities, such as walking and jogging. The values of the power output reached up to 0.5 mW when a temperature difference of about 8.5 °C occurred between the skin and the environment side.

As regards the development of clothing with integrated TEGs, Brogan *et al*. [51] inserted 12 TEGs in a jacket, 6 in the front and 6 in the back side, respectively. In each group consisting of 6 TEGs, the single modules were attached in series between them to increase the voltage output, and then the two groups were linked with a parallel connection to improve the value of the current output. As power output results, the system of 12 TEGs reached up to 0.5 μW in a shady day and

1.25 µW under full sun. Again, by considering a peaked cap as a human garment, Carmo *et al*. [52] developed an autonomous wireless electroencephalogram powered by the human heat energy harvesting. The researchers integrated the TEG and the front-end EEG module in the cap, and they exploited the temperature difference between the forehead and the environment for supplying energy to the device.

Despite a large body of literature focusing on the development and testing of human heat energy harvesting systems, to the author knowledge there is a notable lack of studies targeting the placement of TEGs on the lower limbs.

2.3 NANOGENERATORS FOR HUMAN BODY ENERGY HARVESTING

The results showed in the following section are accepted for publication (July 2017) in:

- ***Trends in Biotechnology*** – *Nanogenerators for Human Body Energy Harvesting*

The newest devices for harvesting the mechanical and thermal energy directly on human body's surface are the nanogenerators (NGs). Their promising properties allow the designing of systems able to maintain the original electronic and structural features also when are bent, twisted and stretched. These remarkable characteristics allow their integration into fabrics, thus having proper contact with the surfaces of the body. Choosing a NG as energy harvester on human body can address the new technological challenge for the development of autonomous systems well suited for the health monitoring of human beings in different application fields, such as the medical science, sport, defense technology and even personal electronic.

In 2006, Wang and Song [53] proposed the first NG prototype, and the rapid growth in this decade was very significant [54]. Up to now, the most common working principles for driving NGs have been piezoelectricity and triboelectricity for transducing biomechanical energy into electricity, while the thermoelectric effect, i.e. Seebeck effect, has been used to transform thermal energy.

The piezoelectric effect relies on the physical and chemical properties of the crystalline phase of the solid matter; if the lattice structure is non-centrosymmetric, the piezoelectric effect may occur under the influence of external perturbations, which produce charge separation across the structure, resulting in electrical polarization of the material.

Instead, a triboelectric NG generates an electrical voltage through frictional contact between solid matters. Contact electrification and electrostatic induction are the physical effects for the generation of triboelectric charges. When two organic or inorganic materials, with different values of electronegativity, come in contact with one another, they generate triboelectric charges on their surfaces, and a voltage difference occurs from the separation of the electrical charges, due to the spatial displacement of materials.

Finally, thermoelectric NGs generate electrical power when a temperature gradient occurs between two dissimilar conducting materials, generally consisting of multiple couples of p- and n-type elements.

2.3.1 PIEZOELECTRIC NANOGENERATORS

A single ZnO nanowire (NW) laterally bonded with silver paste onto a flexible Polyimide (PI) substrate, i.e. Kapton®, has been used first as a piezo-NG to harvest the biomechanical energy on the body surface [55]. The semiconducting property of the ZnO material with metal electrodes at its ends create a Schottky barrier, at least at one end of the NW, thus preserving the piezo-potential in the ZnO-NW and driving the flow of electrons to an external load circuit. In [56], a flexion and extension movement of the index finger resulted in a 0.2% tensile strain onto the structure, generating a piezoelectric potential along the wire. Although the NG-structure was flexible enough to follow the movements of the finger, this prototype showed some disadvantages, such as output stability and mechanical robustness under repeated stress.

In order to increase the robustness of piezo-NG, Lee *et al*. [57, 58] proposed an ultrathin Al-foil to be used both as the substrate and as the electrode for the structure. The prototype enabled detection of wrinkling while fluttering the eyelashes. Another robust configuration for harvesting the biomechanical motion of arm movements relies on the development of an ultrathin ZnO film bonded onto a Polyethylene terephthalate (PET) plastic substrate. The physical properties of the PET allow the mechanical rolling of the whole structure, so that it might be worn at the level of body joints [59]. The only disadvantage of this NG was the brittleness of the Indium tin oxide (ITO) electrode, which limits the rolling curvature of the device to the value of 2 cm. In order to enhance the stretchability of this kind of piezo-NGs, Pradel *et al*. [60] used silicon rubber, i.e. Ecoflex®, for packaging ZnO ultrathin films. This ZnO-NG generates electrical output by transducing the biomechanical movements of the wrist tendons, detecting even the different movements of each finger.

For improved sensitivity and higher resolution in sensing applications, the best piezoelectric elements are polymers. In particular, polyvinylidene fluoride/trifluoroethylene (P(VDF-TrFe)) nanofibres may be aligned together to form piezo-sheets able to harvest biomechanical motion and even detect low pressure values with a resolution of about 0.1 Pa [61]. Park *et al*. [62] proposed a flexible and stretchable P(VDF-TrFe) patch able to detect the movement of the skin due to radial and carotid pulsing, with a displacement resolution of about 1 μm. Both P(VDF-TrFe)-NGs were packaged into an elastomeric matrix of Polydimethylsiloxane (PDMS), which ensures both stability and flexibility for the devices.

All the NGs listed above generate measurable quantities of power output in the range of some nanowatts. In order to increase these power values, many researchers designed NGs made from materials with better piezoelectric properties than those of ZnO and P(VDF-TrFe).

Among the possible piezomaterial alternatives, inorganic PZT and $BaTiO_3$ materials have been introduced: a flexible composite thin film made by P(VDF-HFP) and hemispherical $BaTiO_3$ nanoparticles has been shown to generate a voltage output up to 75 V and a current output of about 15 µA under finger pressure [63]. The hemispherical surface of each nanoparticle enhanced the piezo-power generation thanks to improvements in the surface contact between the active area and the electrode. The entire device, designed onto a PI film, even guaranteed robustness under 2h-long repeated bending cycles. In another application, a flexible piezoelectric PZT thin film developed onto a PET substrate, with interdigitated metal electrodes, harvested energy from the biomechanical movements of the wrist its bending radius value being about 1.6 cm [64-66]; the motion of the wrist produced up to 120 V of voltage output and 2 µA of current output. Finally, Jeong *et al*. [67] proposed the most flexible element for the field of biomechanical energy harvesting: a piezo-elastic-composite made of particles of PMN-PT and multi-walled carbon nanotubes (MWCNTs) packaged in Ecoflex® silicon rubber, which allowed a stretchability of up to 200% of its initial value, generating small quantities of electrical power under the folding movements of the human joints. In order to maintain the robustness of the device, very long Ag-NWs are stretchable electrodes, which ensure high-conductivity and electrical output stability.

2.3.2 TRIBOELECTRIC NANOGENERATORS

At the early stage of the development of tribo-NGs, researchers focused on the design of tribo-NGs composed of a metal plate, positively charged, and a polymeric plate, negatively charged. ***Figure 2B*** shows the triboelectric series for some common inorganic and organic materials.

Concerning biomechanical energy harvesting, Yang *et al*. [68] proposed a tribo-NG backpack able to harvest the energy generated by walking with a 2.0 kg load: multiple polytetrafluoroethylene (PTFE) and Aluminum plates, placed on a flexible PET substrate, operate as tribo-layers and form an integrated rhombic structure.

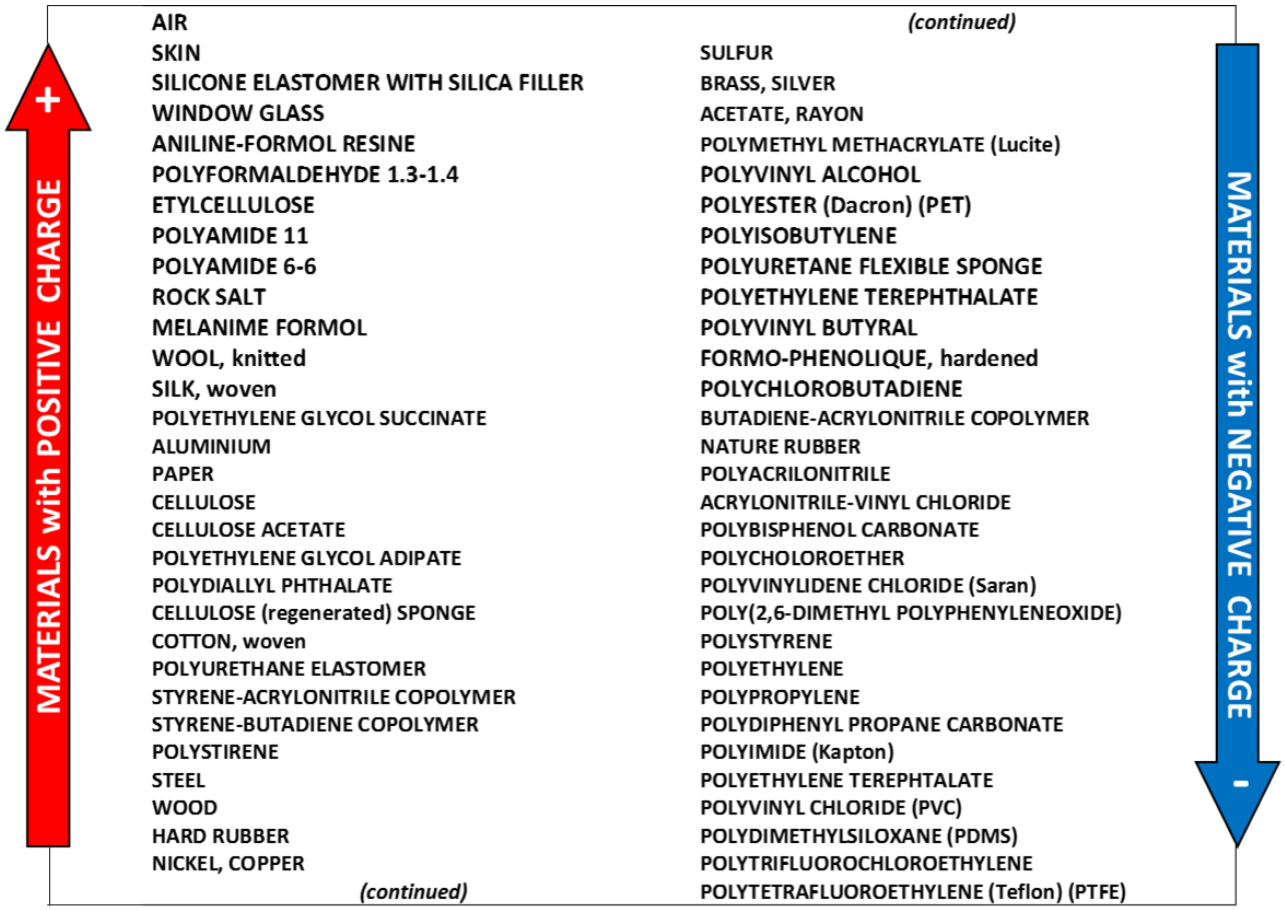

Figure 2B. *Triboelectric series for some common inorganic and organic materials.*

During the contact and release process of the tribo-layers, the NG generates power output in the order of about a milliwatt. Tribo-NGs composed of zigzag structures of multiple PTFE and Al plates were embedded in a shoe insole to generate energy while walking [69, 70]. A patch-NG made of a thin Cu cantilever spring sandwiched into a folded CPP film detects the body movements during sleep, without needing an external power source [71]. Concerning these latter NGs, the power output strongly depends on the good adhesion between the two active layers. Modifying the tribo-layers by adding surface porosity or by implementing micro-cubic or micro-pyramid array structures [72, 73], the power output increases, and may be able to reaching values in the hundreds of volts and hundreds of microamperes.

The polymeric physical state of tribo-layers allows for greater flexibility than the metal-based ones, although at the expense of a lower power output. The stretchability of NGs even depends on

the nature of the electrodes: ITO electrodes are the most widely used for transparent conducting film in tribo-NGs, which mainly operate under compressive stress, but their brittle nature does not allow for the withstanding of high tensile strain. Therefore, conducting polymers and metal or carbon nanostructures are alternatives to ITO electrodes for developing stretchable devices [74]. In particular, Yang *et al*. [75] developed an imperceptible and stretchable tribo-NG for harvesting the biomechanical energy of human joint movements. The tribo-NG consisting of a wavy Kapton® film sandwiched between two Cu serpentine electrodes on a PDMS substrate supports a tensile strain of up to 22%, making the NG-structure suitable to be attached to the skin. Again, to increase the stretchability of tribo-NGs, Hwang *et al*. [76] proposed a device composed of two polymeric tribo-layers and very long Ag-NW electrodes. In such a way, the NG withstands tensile strains of about 40%, while breathing, coughing and swallowing, among many other human physiological activities.

As a basic structure of all the tribo-NGs listed above, two electrodes are mandatory for proper device operation, but in some cases they may limit the application fields and increase development costs. A single-electrode mode can overcome these limitations, and it expands the applicability of tribo-NGs in the research field of biomechanical energy harvesting and human-machine interfacing. According to the tribo-series [77], human skin is a triboelectric layer, which presents electrostatic charges on its surface once it is in contact with dielectric or ferroelectric materials [78]. PDMS polymer film is widely used as friction layer for developing tribo-NGs, which involve the skin layer in the generation of tribo-charges. In the scientific literature, these NGs work as self-powered tactile sensors for tracking the location, velocity and force of human touch [79-81]. In addition, tribo-NGs based on the friction contact between the epidermis and PDMS polymer can monitor human motion, by measuring the angle displacements of the main body joints [82-84]. However, the PDMS polymer may be not suitable for following all movements of the limbs, due to its elongation limit. Thus, Lai *et al*. [85] developed a tribo-layer made of Ecoflex® silicon rubber, in

which Ag-NWs were dispersed internally, to form a stretchable electrode. This tribo-NG sustains tensile strains of over 300%, making the device highly conformable for electronic-skin applications.

2.3.3 THERMOELECTRIC NANOGENERATORS

Bi_2Te_3 and Sb_2Te_3 are the conventional n- and p- type elements for developing the multiple thermocouples constituting the thermo-NGs, thanks to their high thermoelectric efficiency at room temperature. However, the brittle nature of these inorganic compounds does not allow for flexibility of the NGs, so it makes it necessary to use polymeric materials for supporting and packaging the thermoelectric elements to impart the desirable flexibility to the NG-structure.

A flexible thermo-NG adheres to the body surface better than a rigid one, optimizing the thermal conductance between the skin and the generator, thereby increasing the temperature difference between the hot and cold sides of the NG. For example, Hyland *et al*. [86] wrapped a rigid thermo-NG into a PDMS polymer, increasing the device area, but conferring a minimum of flexibility for the entire structure. In this way, the NG was easily placed on the chest and the researchers tested the performance of the device under different walking speeds. In order to enhance the device flexibility, Jo *et al*. [87] designed a PDMS polymer substrate with several holes which were filled by columns of thermoelectric elements. The entire structure comprises eight p-n junctions in 250 mm^2, with a thickness of more than 4 mm, which does not allow for large bending movements.

To enhance thermo-NG flexibility, We *et al*. [88] proposed a hybrid composite thermo-NG, by infiltrating an organic conducting polymer, the PEDOT:PSS, into the pores of an inorganic thermoelectric film. The minimum value of the NG bending radius was about 3 cm, so that it could be worn on the wrist. In addition, this NG supports over 1000 cycles of bending movements without showing signficant degradation in output performance. Another example of a flexible thermo-NG is the wavy-shape module presented by Francioso *et al*. [89, 90]. The researchers assembled the p- and n-thermolegs on a wavy substrate made of two PDMS layers covered with a thin layer of

Kapton®. The former PDMS layer was Ag-filled to enhance the contact between the skin and the hot thermo-junctions, while the latter insulates the cold junctions from the hot ones. This wavy-shape NG counts up to 2778 p-n thermocouples and generates 250 mV when the temperature gradient is about 5 K. This voltage output value is very high for the field of energy harvesting by body heat; however, the authors performed just simulation tests.

2.3.4 FABRIC NANOGENERATORS

NGs based on fabrics can represent a significant innovation for harvesting energy directly on the body surface, as humans wear clothes at each moment of the day. In particular, fabrics made of polymeric materials are very common in the textile market thanks to their low-cost large-scale manufacturing. Therefore, adding an active polymer into common fabrics could represent a new trend in developing smart-clothes for harvesting energy. Among all the working principles for designing NGs, the triboelectric one is the most used because it relies on the contact/release process of any materials with different electronegativity values; as opposed, instead, to piezoelectric and thermoelectric ones, which depend on the physical and chemical properties of the chosen active elements for harvesting the energy. For example, NGs based on piezoelectric fabrics should be flexible and almost stretchable, and only the PVDF polymer ensures both these features. Zeng *et al*. [91] proposed a wearable NG made of PVDF-$NaNbO_3$ nonwoven fabric as the active material, and conductive yarns as electrodes. This NG works under compressive stress and shows great stability also over 1,000,000 compression–release cycles, which is a value higher than a NG made of only $NaNbO_3$-NWs elements [92]. PVDF monofilaments can be also “3D-spacers” between two knitted layers made of nylon yarns, thus having an all-fibre NG [93]. The technologies for knitting 3D-spacer fabrics are highly used in the textile industry, therefore this example of piezo-NG can open the way for clothes to be easily designed for harvesting energy.

Regarding the design of textile-based NGs, which exploit the triboelectric effect, nylon fabric represents a good choice as a contact layer for the generation of energy when it rubs against polymeric materials, such as PDMS [94], PTFE [95], fluorinated ethylene propylene [96, 97] and polyester (PES) [98], among many others. Again, denim fabric in the contact/release process with PI represents a tribo-NG well-suited for harvesting biomechanical energy [99]. However, these fabric NGs do not rely on knitting techniques, but rather they seem to be single or multiple patches assembled on fabrics. Thus, Liu *et al*. [100] proposed a tribo-NG textile without a multilayered structure, where PET fibres interlace at the top surface of the fabric and penetrate across its thickness on the bottom side, so the final structure looks like a three-dimensionally penetrated fabric. Again, Zhao *et al*. [101] fabricated a textile tribo-NG by weaving Cu-coated PET (Cu-PET) warp yarns and PI-coated Cu-PET weft yarns. This NG shows washability capability, resulting in its suitability for common daily use. However, to have greater stretchability, a conductive polymer should replace the Cu metallic material.

Developing thermo-NGs based on fabric structures is very difficult since the brittle nature of the inorganic thermoelectric elements does not allow for their integration into textiles. However, Lu *et al*. [102] deposited thermoelectric p-n columns on both sides of a silk fabric. In this way, the NG supports multiple bending and twisting movements, thus opening the possibility to integrate thermo-NGs into clothes. Again, by using a sewing process, Kim *et al*. [103] utilized conductive fabric threads for electrically connecting in series the thermo-columns into a PI substrate. Then, the entire structure was sewn into a t-shirt for harvesting thermal energy while walking. In addition, Siddique *et al*. [104] proposed a similar structure, composed of PES fabric as substrate, Ag-threads as a conductive element, and p- and n-types Bi_2Te_3 as thermoelectric elements. The textile and flexible thermo-NG can easily wrap the forearm for harvesting thermal energy also in harsh environments. Finally, by coating commercial fabrics with PEDOT:PSS polymer it is possible to develop flexible and

foldable thermo-NGs. Although such a polymer properly works in a temperature range of about 300 - 390 K, which may be compatible with human activities, the voltage output is too low for considering this NG as being able to harvest human thermal energy [105].

2.4 TEXTILE SENSORS FOR BIOMECHANICAL SENSING

Textile sensors are a recent technology for sensing the biomechanical movements of the human body. Since at the end of '90s, De Rossi *et al*. [106] outlined the guidelines regarding the study of the conductive polymers properties placed on textiles for strain and temperature sensing, many researchers deepened this technology for clinical and wellness purposes, among many others. For example in 2002, Edmison *et al*. [107] described the desirable characteristics of the piezoelectric materials for the field of wearable electronic textiles. They proposed a glove that employed piezoelectric elements to sense the movements of the hand. In 2004, Lorussi *et al*. [108] developed an elastic lycra fabric coated with a thin layer of polypyrrole (PPy) for developing a conducting fabric. As sensing elements, many strain gauges were deposited directly onto the fabric and so, they proposed a sensing sleeve for the arm posture detection, a textile kneepad for monitoring the movement of the leg and a sensing glove for the recognition of a power grasp. A year later, the same group of researchers developed newly strain sensors based on rubber-carbon-coated threads for designing smart fabrics. The fabric was used for the assessment of breathing and for the monitoring of motion activities. In addition, they developed electrodes based on metal conductive threads for detecting bioelectrical signals, such as the electrocardiogram (ECG) and the electromyogram (EMG) [109]. For the recording of the ECG signal, Cho *et al*. [110] developed electrodes with stainless steel yarns, for integrating them into clothing. They found that electrodes using metallic embroidering are more efficient when its substrate was a metal blended fabric. The electrolessly Cu/Ni plated fabrics obtained the best values of conductivity for the electrodes based on textiles.

As regards the clinical purposes, Tesconi et al. [111] developed a new generation of garments by using conductive elastomer composites with piezoresistive properties. The garments were deposited over a sub layer of cotton Lycra for developing a smart leotard to provide an unobtrusive technique for identifying the clinical stage of the recovery process of patients affected by venous ulcer. Again, O'Quigley *et al*. [112] proposed a solution for the home-monitoring of patients who suffer of rheumatoid arthritis, by using a smart glove based on piezoresistive fabrics. In this way, the patients used the glove to perform daily exercises prescribed by the doctor and thus, the doctor could monitor their rehabilitative progress from the clinic. In another study, Rai *et al*. [113] studied the use of nanosensors embedded into textiles for the health monitoring of neurological and cardiovascular disorders.

As regards the monitoring of the trunk motion, Mattmann *et al*. [114] developed a garment prototype for the recognition of twenty-seven upper body postures. As sensing element, they used a commercial thermoplastic elastomer filled with carbon black powder. The garment changed its resistivity value by length deformations. Again, Coyle *et al*. [115] developed a fabric based sensor for collecting the value of the pH, in order to analyze the sweat secretion during sport exercises, and Lee *et al*. [116] evaluated the piezoelectric polymers as sensing elements in smart textiles for monitoring the vital signals and for the evaluation of the energy expenditure of people. Moreover, Ozdemir and Kilinc [117] developed a fabrics able to measure the bio thermal variable of human beings, by soldering temperature sensors on conductive threads coated with cotton.

As regards the monitoring of the angle variations of the main body joints, Hu *et al*. [118] proposed a conductive fabric coated with polypyrrole (PPy) for the human joint angle monitoring, and Muthukumar *et al*. [119] analyzed the behavior of fabrics coated by polyaniline (PANI) for measuring the elbow angle variations. In addition, Shyr *et al*. [120] developed an elastic conductive

webbing for monitoring the flexion angle during the elbow and knee movements and Tognetti et al. [121] proposed a new generation of wearable goniometers based on knitted piezoresistive fabric. Finally, regarding the possibility to enhance the stretchability of devices, Menguc *et al*. [122] developed a soft sensing suit for monitoring ankle, knee, and hip angle joints, by using a hyper-elastic strain sensor based on microchannels of liquid metal, the eutectic gallium indium alloy (eGaIn). The sensor was embedded into an elastomer substrate. Again, Kramer *et al*. [123] introduced a curvature sensor made of microchannel of eGaIn liquid onto an elastomer film substrate for the proprioception of joint angles, and again, Yoon *et al*. [124] reported a new class of strain sensors by combining the merits of microfluidic systems with ionic liquids.

ENERGY HARVESTING FROM HUMAN HEAT (C)

3.1 HUMAN BODY THERMAL CHARACTERISTICS AND ENVIRONMENTAL ASPECTS

From an energy perspective, the human body is a rich and lasting energy source, since it is a permanent heat release unit. It follows naturally, to try to harness this wasted energy for powering wearable devices [20].

Several factors affect the performance of the systems for harvesting the thermal energy on human body, and their study is imperative to do an accurate analysis about the real possibilities of recovering this kind of energy.

The human body physiological parameters and the environmental conditions are the main factors that affect the performance of the energy harvesting system, and they are summarized as follows. At first, it is important denote the physical characteristics of the living tissues, such as the thickness of the fat layer, the depth of the muscles tissue and the anatomy of the skin surface. Then, the diameter, the position and the number of the subcutaneous blood vessel are relevant physical features to determinate the temperature of the body surface. Once again, it is important consider the physiological state of the body, represented by the metabolism, blood perfusion and sweat secretion, and finally, the main environmental parameters are the air temperature and air [125].

As regards the physical characteristics of the living tissue, the ***Figure 1C*** shows a simplified three-layer model of the body tissue, consisting of muscle tissue, fat layer and skin surface.

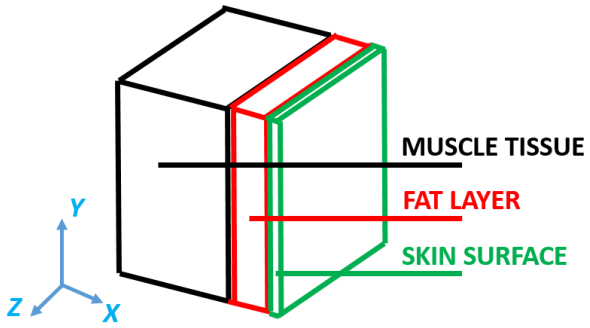

Figure 1C. *A simplified three-layer model of the body tissue, consisting of muscle tissue, fat layer and skin surface.*

In order to characterize the heat transfer between the tissues of the human body, the *Pennes bioheat equation* describes the influence of the blood flow on the temperature distribution among such tissues [126]. *Equation (1C)* shows the Pennes's formula, concerning Cartesian coordinates:

$$(1C): \qquad \rho c \frac{\partial T(X,t)}{\partial t} = \nabla k(X)\, \nabla[T(X,t)] + Q_b + Q_m\,, \qquad X \in \Omega$$

where, X contains the Cartesian coordinates x, y and z; Ω represents the living tissue; $T(X,t)$ is the tissue temperature distribution; $k(X)$ is the space-dependent thermal conductivity of the tissue and finally, ρ and c are the density and specific heat of the tissue. Q_m is the metabolic heat generation rate and Q_b is the blood heat generation rate, defined as follows in *equation (2C)*:

$$(2C): \qquad Q_b = \rho_b c_b \omega_b(X)[T_a - T(X,t)]$$

where $\omega_b(X)$ is the space-dependent blood perfusion, ρ_b and c_b denote the density and specific heat of the blood and finally, $T_a$is the arterial temperature, often treated as a constant. In the present model, the blood perfusion and the rate of the metabolic heat generation exist only in the muscle tissue.

In numerical calculations, the typical values for the parameters of the living tissues are the following [127]:

- $\rho = \rho_b = 1000\ \frac{kg}{m^3}$;

- $c = c_b = 4200\ \frac{J}{kg\ K}$;
- $k_{muscle} = 0.5\ \frac{W}{m\ K}$;
- $k_{skin\ surface} = 0.3\ \frac{W}{m\ K}$;
- $k_{fat} = 0.2\ \frac{W}{m\ K}$;
- $k_{sweat\ secretion} = 0.6\ \frac{W}{m\ K}$;
- $Q_m = 420\ \frac{W}{m^3}$;
- $\omega_b = 0.0005\ \frac{mL}{s\ mL}$;
- $T_a = T = 37\ °C$.

As regards the effects of the environmental conditions, which influence the heat transfer between living tissue and the environment, the most critical parameters are the air temperature and air humidity and the heat transfer coefficient between living tissue and the. Generally, the lowest air temperature and the highest value for the heat transfer coefficient lead to have the best situation for harvesting the wasted thermal energy on human body.

In daily life activities, numerous physiological states of the body occur by performing different activities, such as working at the desk rather than doing sport exercises. For example, blood perfusion and metabolic heat generation, which have a significant effect on the temperature distribution in biological bodies, significantly increase when a person is taking multiple physiological activities. As a result, the most suitable situation for harvesting the human thermal energy is when the body is under an excited physiological state. Finally, the sweat secretion is the most important parameter for the body temperature regulation, since it leads to have a balanced temperature inside the body. When high values of the temperature difference between the skin and the environment occur, the sweat secretion tends to reduce this temperature difference, so balancing the normal physiological parameters.

Therefore, the skin temperature is non-uniform on the body surface. ***Table 1C*** shows the main values of the skin temperature for different body locations. The results are summarized based on the works proposed by Yang *et al*. [128], Zaproudina *et al*. [129] and Webb [130]. The first two authors measured the temperature of the skin by using the infrared thermography technology, while Webb collected the body temperature data by using a probe with thermistors. Again, Yang *et al*. acquired the data at a room temperature of 17.5 °C, Zaproudina *et al*. made the measurements at 23.5 °C of air temperature and Webb proposed the results with an environmental temperature of 27 °C.

Table 1C. *Skin temperature for different body locations.*

Main body parts	**Yang *et al*. [128]** **(T_{air} = 17 °C)**	**Zoupradina *et al*. [129]** **(T_{air} = 23.5 °C)**	**Webb [130]** **(T_{air} = 27 °C)**
FOREHEAD	29.5 °C	34.1 °C	35.2 °C
NECK	31.1 °C	33.2 °C	35.1 °C
BACK	30.6 °C	32.5 °C	34.4 °C
CHEST	30.3 °C	32.3 °C	34.4 °C
ARM ANTERIOR	30.3 °C	31.7 °C	33.2 °C
FOREARM	29.5 °C	31.5 °C	34.0 °C
THIGH	28.3 °C	30.8 °C	33.0 °C
CALF	29.4 °C	31.3 °C	31.6 °C
FOOT DORSAL	27.1 °C	28.6 °C	30.4 °C

The data in ***Table 1C*** refer to the main body parts, such as the forehead, neck, upper back, chest, arm anterior, forearm, thigh, calf and foot dorsal. From these data, it results clear that the

body temperature increases with the highest environmental temperatures. By 10 °C rise of the air temperature, the skin temperature increases on average of about 4 °C.

3.2 TECHNIQUES FOR HARVESTING THE HUMAN HEAT ENERGY

The application field of human heat energy harvesting concerns the recovery of dissipated body heat, by exploiting the thermoelectric effect. The thermoelectric effect implies a voltage generation across two dissimilar metals or semiconductors when a temperature difference occurs between them. In 1821, T. J. Seebeck discovered this phenomenon, so became known as Seebeck effect [131]. A quantitative constant describes the Seebeck effect, and *equation (3C)* define it, the Seebeck coefficient, as follows:

$$(3C): \qquad \alpha = -\frac{\Delta V}{\Delta T}$$

where ΔV is the electrical voltage difference, and ΔT is the value of the temperature difference between the two dissimilar metals or semiconductors. Generally, α is measured in $\mu V/K$.

In the middle of the 20th century, the scientists around the world deepened the study about the semiconductors behavior as thermoelectric elements, thus creating the first thermoelectric generator (TEG). A TEG consists of multiple p- and n-type semiconductor elements alternating each other and two metal conductors, electrically connect them in series. Again, in order to create a TEG module, two ceramics plates encapsulate the series of thermoelectric elements for the electrical insulation, but making the TEG thermally conducting.

The thermoelectric figure of merit (ZT), denotes the energy conversion efficiency of thermoelectric materials. It is a dimensionless quantity, and *equation (4C)* define it, as follows:

$$(4C): \qquad ZT = \frac{\sigma \alpha^2 T}{\kappa}$$

where α is the Seebeck coefficient, T is the average temperature and finally, σ and κ are the electrical and thermal conductivity of the materials, respectively. In order to define the working efficiency of TEG modules, *equation (5C)* combines the figure of merit ZT and the expression for the definition of the Carnot cycle ($\frac{T_H - T_C}{T_H}$):

$$(5C): \qquad \eta = \frac{T_H - T_C}{T_H} \frac{\sqrt{1+ZT}-1}{\sqrt{1+ZT}+\frac{T_C}{T_H}}$$

where η can assume a value between zero and one. The ZT value is the most critical parameter for the performance of the thermoelectric generator. In today's best commercial TEGs, ZT is about 1 at 25°C [132]. It means that TEGs operate at only 10% of the Carnot efficiency [133]. Some 30% of Carnot efficiency, comparable to home refrigeration, could be reached by a TEG module with a ZT value equal to 4, but this value is too hard to achieve nowadays [134].

Figure 2C shows the structure of a TEG module and its equivalent, simplified electrical circuit.

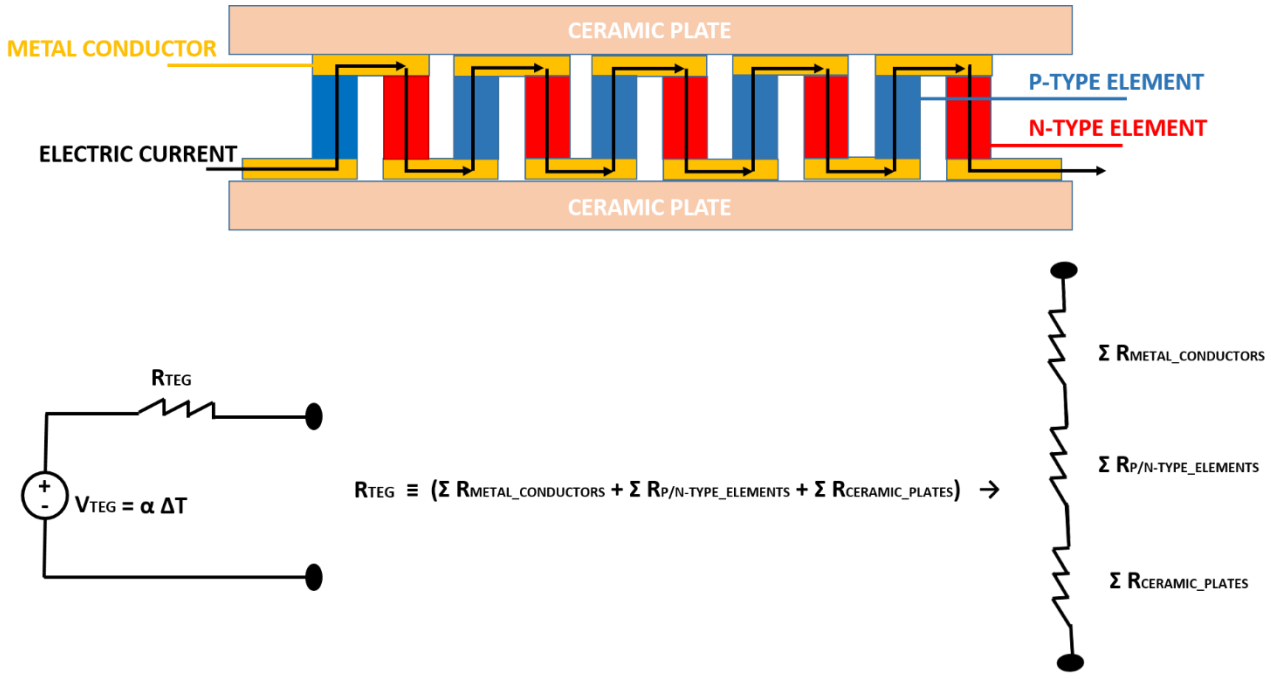

Figure 2C. *Structure of the TEG module and its equivalent, simplified electrical circuit.*

In ***Figure 2C***, a voltage source in series with an internal resistance (R_{TEG}) represents the simplified electrical circuit for the TEG module. The TEG produces an electrical current flow in an external circuit by the imposition of a temperature difference (ΔT) between its two sides. The amplitude of the ΔT determines the magnitude of the TEG voltage (V_{TEG}) and, the direction of the heat flow determines the voltage polarity. Furthermore, a change of ΔT across the TEG causes a variation of the value of its internal resistance, R_{TEG} [135]. So, in the application field of the heat energy harvesting on human body, it is extremely hard having a stable value for R_{TEG}, since the temperature across the two sides of TEG continuously changes, based on the physiological state of the body and from the external environmental conditions.

Figure 3C shows the circuit to measure the electrical power delivered by the TEG.

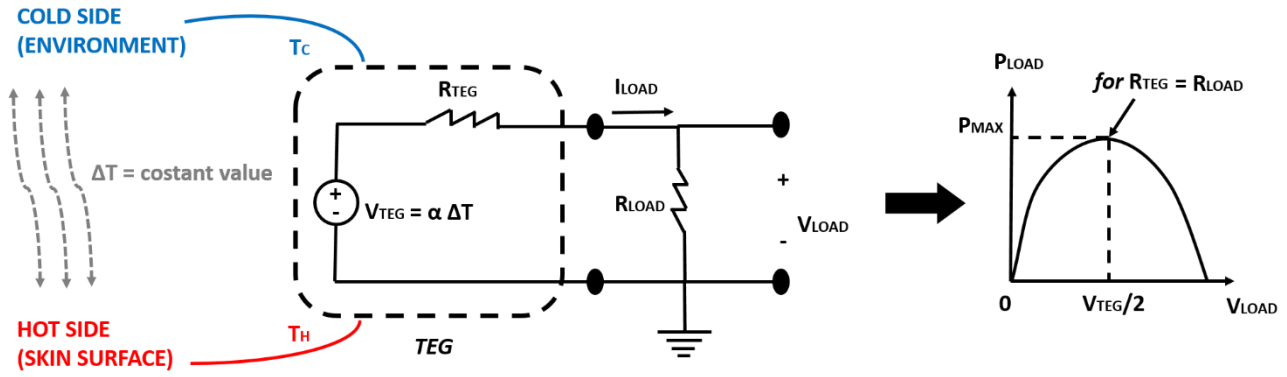

Figure 3C. *Electrical circuit for the measurements of power delivered by the TEG, with the corresponding power track versus the closed circuit voltage.*

For a given temperature difference between the two sides of TEG, the value equals to the half the open circuit voltage ($V_{TEG}/2$) gives the corresponding maximum value of the power output (P_{MAX}) and at this point, the electrical load impedance (R_{LOAD}) should be equal to the value of the TEG internal resistance (R_{TEG}) [136]. *Equation (6C)* and *(7C)* describe the calculus to demonstrate the curve in ***Figure 3C***:

$$(6C): \qquad V_{out} = V_{TEG}\frac{R_{LOAD}}{R_{TEG} + R_{LOAD}} \quad \Leftrightarrow \quad P_{OUT} = \frac{V_{OUT}^2}{R_{LOAD}}$$

$$(7C): \qquad \frac{dP_{OUT}}{dR_{LOAD}} = \frac{d\left(\frac{V_{OUT}^2}{R_{LOAD}}\right)}{dR_{LOAD}} = 0 \quad \Leftrightarrow \quad R_{LOAD} = R_{TEG}$$

3.3 EXPERIMENTAL SECTION

3.3.1 THERMOELECTRIC GENERATOR CHOSEN

A TEG generates measurable electrical energy when a temperature difference occurs between its two sides, e.g., Seebeck effect. Thanks to this property, a TEG that adheres to the surface of human skin can produce electrical power by transducing the wasted body-heat energy. ***Table 2C*** lists the main features of the TES1-12704 module and the ***Figure 4C*** shows the TES1-12704 TEG module [137].

Table 2C. *Properties of the TES1-12704 module*.

Properties	**TES1-12704**
Dimensions (l x w x t), (mm)	(30 x 30 x 3.2)
Weight, (g)	0.015
Ceramic substrate material	Aluminum oxide (Al_2O_3)
Metal conductors material	Copper (Cu)
Number of p-n couples	127
p- and n- type elements material	Bismuth telluride (Bi_2Te_3)
Electrical conductivity, σ (1 / cm Ω)	800 – 1350
Thermal conductivity, κ (W / cm K)	0.016 – 0.02
Seebeck coefficient, α (μV / K)	160 – 200
Coefficient of merit, Z (1 / K)	0.002695 – 0.003

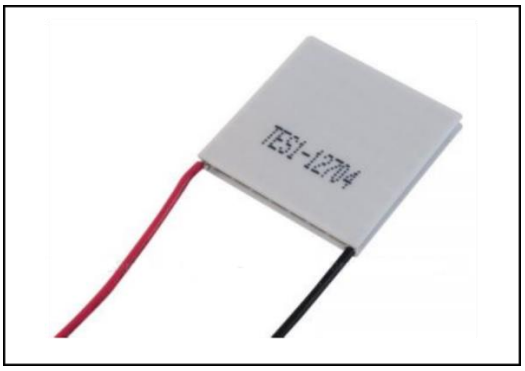

Figure 4C. *The TES1-12704 module.*

3.3.2 TEG PLACEMENT ON HUMAN BODY and PERFORMED ACTIVITIES

The placement of the TEG on human body occurred on four body positions, two in the upper part and two in the lower one, respectively.

In order to easily wearing the TEG onto the skin, the four chosen body parts were the large skin areas corresponding to the superficial muscles of arm and leg. The biceps brachii in the arm anterior and the flexor carpi radialis in the forearm were the muscles corresponding to the placement of the TEG in the upper body part, while the gracilis in the thigh and the gastrocnemius in the calf were the chosen muscles for placing the TEG on the leg.

Three human daily activities, such as sitting to rest, walking and jogging were the performed test exercises. For the resting activity, the placement of the TEG occurred in all the four skin areas corresponding to the superficial muscles mentioned above. Instead, for the walking and jogging activities the placement of the TEG took place only onto a subset of the aforementioned ones: the biceps brachii and the gastrocnemius.

3.3.3 A FABRIC BAND TO SUPPORT THE TEG

In order to place the TEG directly onto the skin surface, a fabric band acted as support for the TES1-12704 module. The PVC fabric and the gauze were the materials of the proposed band. ***Figure 5C*** shows a picture of the two fabric materials.

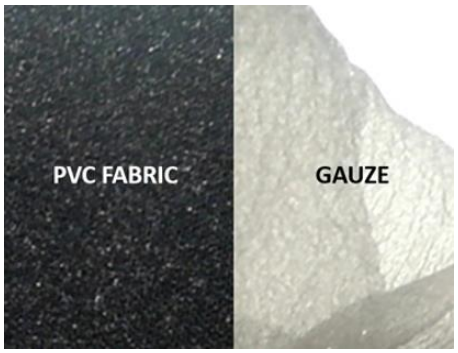

Figure 5C. *A picture of the PVC fabric on the left and the gauze for clothing in the left.*

The PVC fabric is a nonwoven fabric made up of a group of long fibers with a random pattern. It guarantees excellent thermal insulation and so, it was the bottom layer of the band in order to thermal insulate the contact area between the skin and the TEG. Conversely, the gauze is a structure with a loose open weave. It is a thin netting, translucent fabric, with a good feature of breathability. Based on these characteristics, it is used as the top layer of the band.

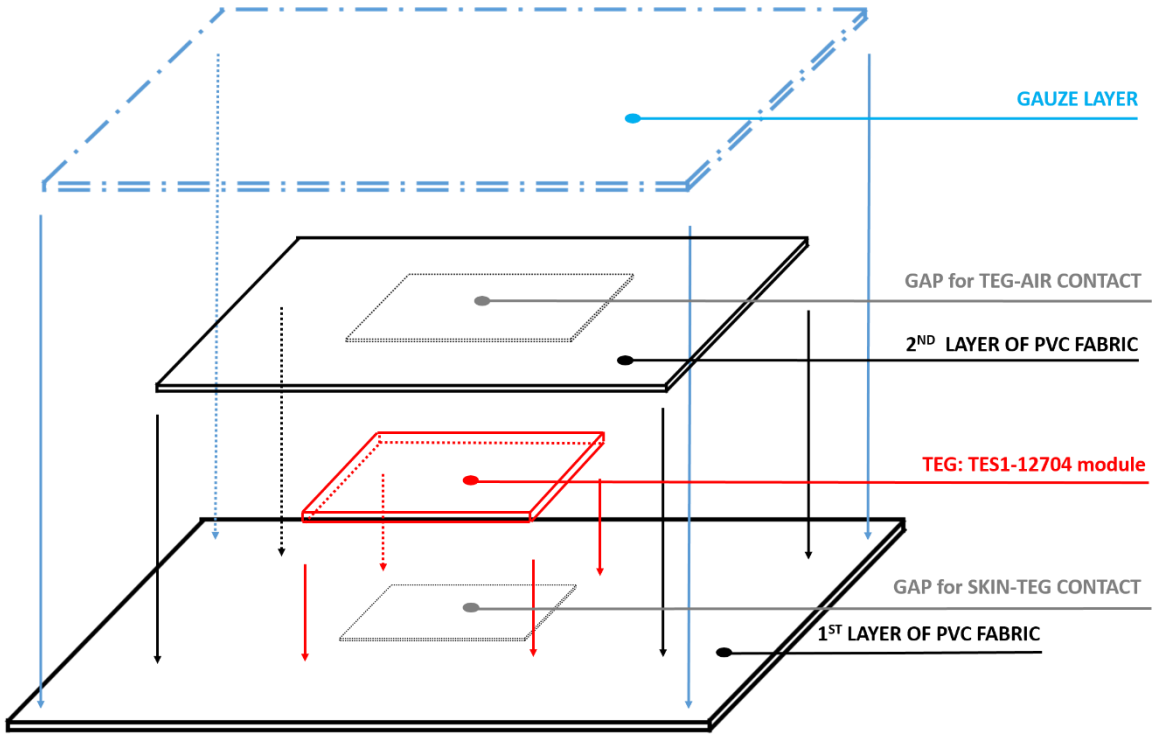

Figure 6C. *The fabrication process of the support fabric band.*

Figure 6C shows the fabrication process of the support band. At first, the PVC fabric was cut to form a rectangular sheet with area size of about 350 cm^2, and a gap for the contact area between the skin and the TEG was made by cutting the PVC sheet in its central part. The square hole had an area size of about 2.5 cm x 2.5 cm. Therefore, the TEG with surface area of 3 cm x 3 cm was encapsulated between the mentioned PVC sheet and a second PVC layer, which was also with a hole in its central part, but with a greater size area (2.9 cm x 2.9 cm) than the first one. Finally, a transpiring layer, made from gauze was placed onto the PVC fabric layers and TEG, for enhancing the stability of the system, but not thermally isolating the TEG from the external environment. All the fabric layers were knitted by using cotton yarns. To conclude the support band, four laces were sewn on its ends.

3.3.4 EXPERIMENTS AND DATA DISCUSSION

Figure 7C shows the measurement circuit to find out the values of the voltage output generated by the TEG. These values were measured and acquired by the NI-USB-6210 data acquisition system (DAQ), National Instruments.

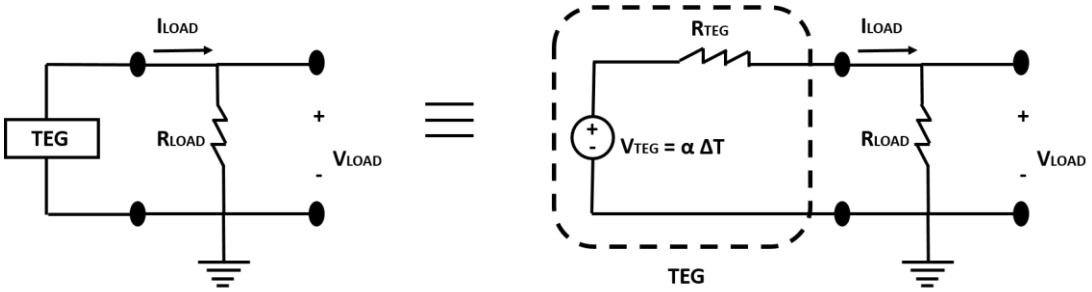

Figure 7C. *TEG measurement circuit.*

The voltage output for the circuit in ***Figure 7C*** is given by the *equation (6C)*, mentioned in the above section, so as the *equation (7C)* to find out the values of the power output.

Two stages of the performed activities were the experimental tests for the proposed energy harvesting system. In the former one, two healthy male volunteers (age: 27 ± 3 years; body weight: 74 ± 1 kg; height: 175 ± 5 cm) stayed in resting position for more than 20 minutes, during which the

voltage values were acquired in accordance to the following temporary intervals: at the 1st minute, then at the 5th minute, again at the 10th minute and finally at the 20th minute. Instead, in the latter one, four healthy male volunteers (age: 25 ± 5 years; body weight: 69 ± 10 kg; height: 174 ± 6 cm) performed for three times the following cycle of multiple activities: at first, 2 min of sitting position, then 2 min of walking activity, again 2 min of sitting position and 2 min of jogging activity and finally, 2 min of sitting position, once again.

As regards to the first stage of the experimental tests, the measurements were made to find out the value of the resistive load, which maximizes the power output. Thus, the voltage data were acquired in varying the external load from the values range 1 – 32 Ω. Particularly, the range of the values of the resistor load was as follows: 1.12 Ω, 3.88 Ω, 4.68 Ω, 5.71 Ω, 7.61 Ω and 31.84 Ω.

In addition, in order to measure the temperature difference across the TEG, two ultrathin thermocouples were attached on both sides of the TES1-12704 module, by using an elastic sport tape. In such a way it was possible compare the occurred temperature difference between the two sides of the TEG and the power generated through the performed resting position. The controlled room temperature was about 25 °C.

***Figure 8C*-(a)** shows the power output generated by the TEG when it was on the arm anterior, in correspondence to the biceps brachii muscle, while ***Figure 8C*-(b)** shows the relative temperature difference across the TEG during the experiment.

In the diagram of ***Figure 8C*-(a)** the power output reached up to 5 μW after 1 minute of the performed test, and it decreased up to 4 μW at the end of the measurements. This variation of about 1 μW depended on the decreasing of the temperature on both sides the TEG. As it can be clearly seen in ***Figure 8C*-(b)**, it decreased from 2.25 °C to 2.00 °C.

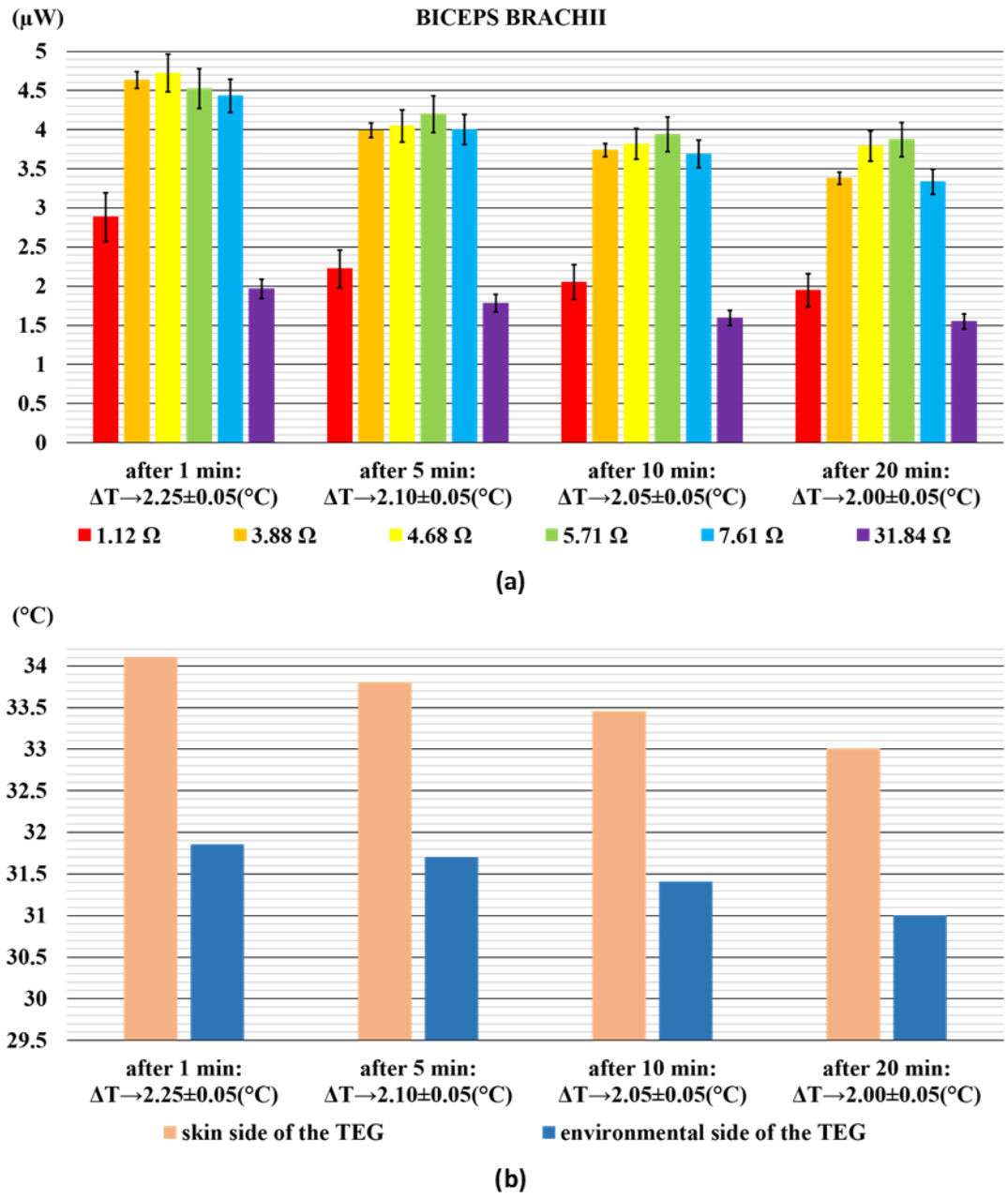

Figure 8C. *The power output generated by the TEG on the arm anterior, in correspondence to the biceps brachii* **(a)** *and the relative temperature difference* **(b)**.

***Figure 9C*-(a)** shows the power output generated by the TEG when it was on the forearm, in correspondence to the flexor carpi radialis muscle, while ***Figure 9C*-(b)** shows the relative difference of temperatures between the skin and the air-environmental side of the module.

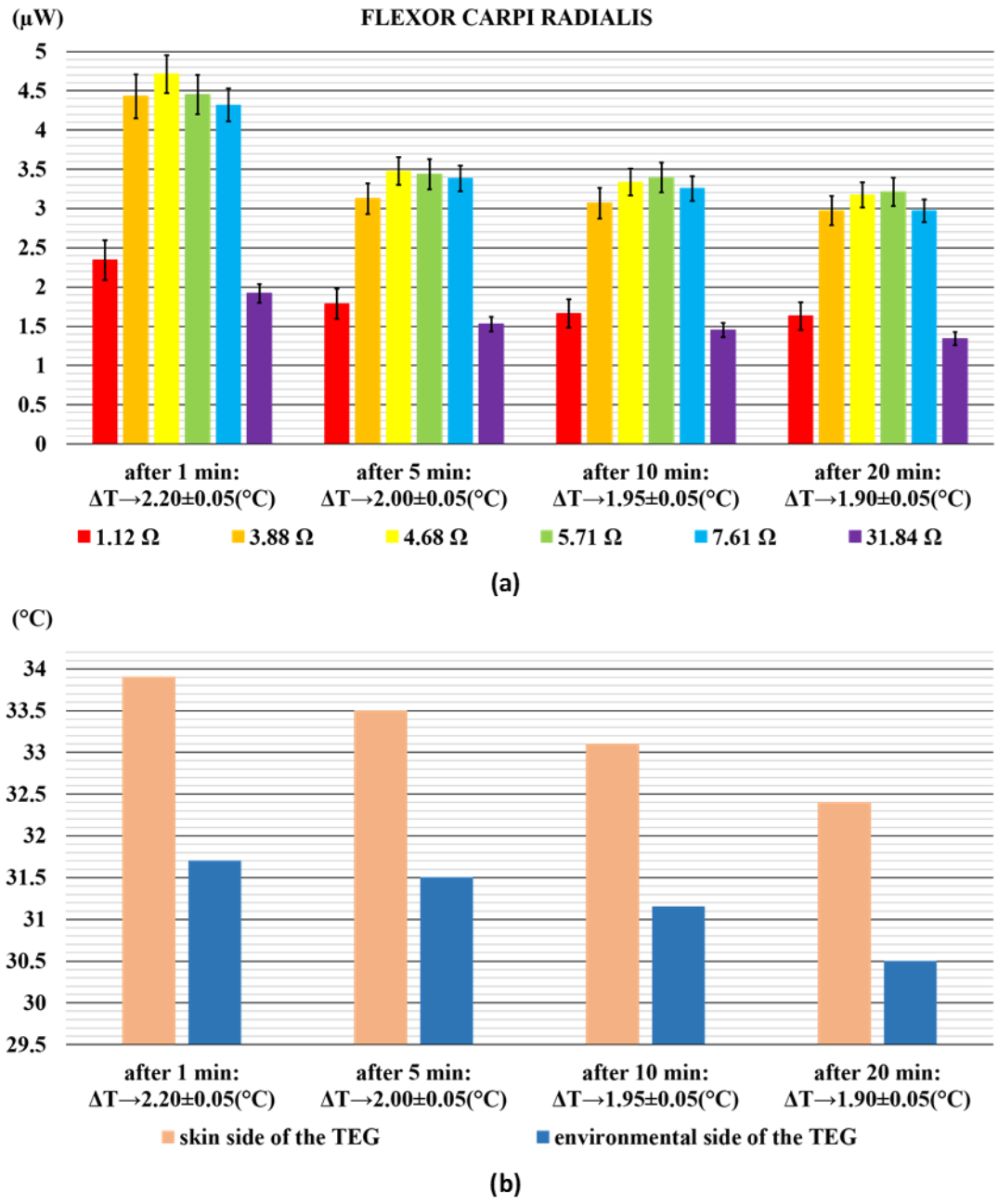

Figure 9C. *The power output generated by the TEG on the forearm, in correspondence to the flexor carpi radialis* **(a)** *and the relative temperature difference* **(b)**.

In the diagram of ***Figure 9C*-(a)** the power output reached up to 4.8 μW after 1 minute of the performed test, and it decreased up to 3.3 μW at the end of the measurements. This variation of about 1.5 μW depended on the decreasing of the temperature on both sides of the TEG. As it can be clearly seen in ***Figure 9C*-(b)**, it decreased from 2.20 °C to 1.90 °C.

***Figure 10C*-(a)** shows the power output generated by the TEG when it was on the thigh, in correspondence to the gracilis muscle, while ***Figure 10C*-(b)** shows the relative difference of temperatures between the skin and the air-environmental side of the module.

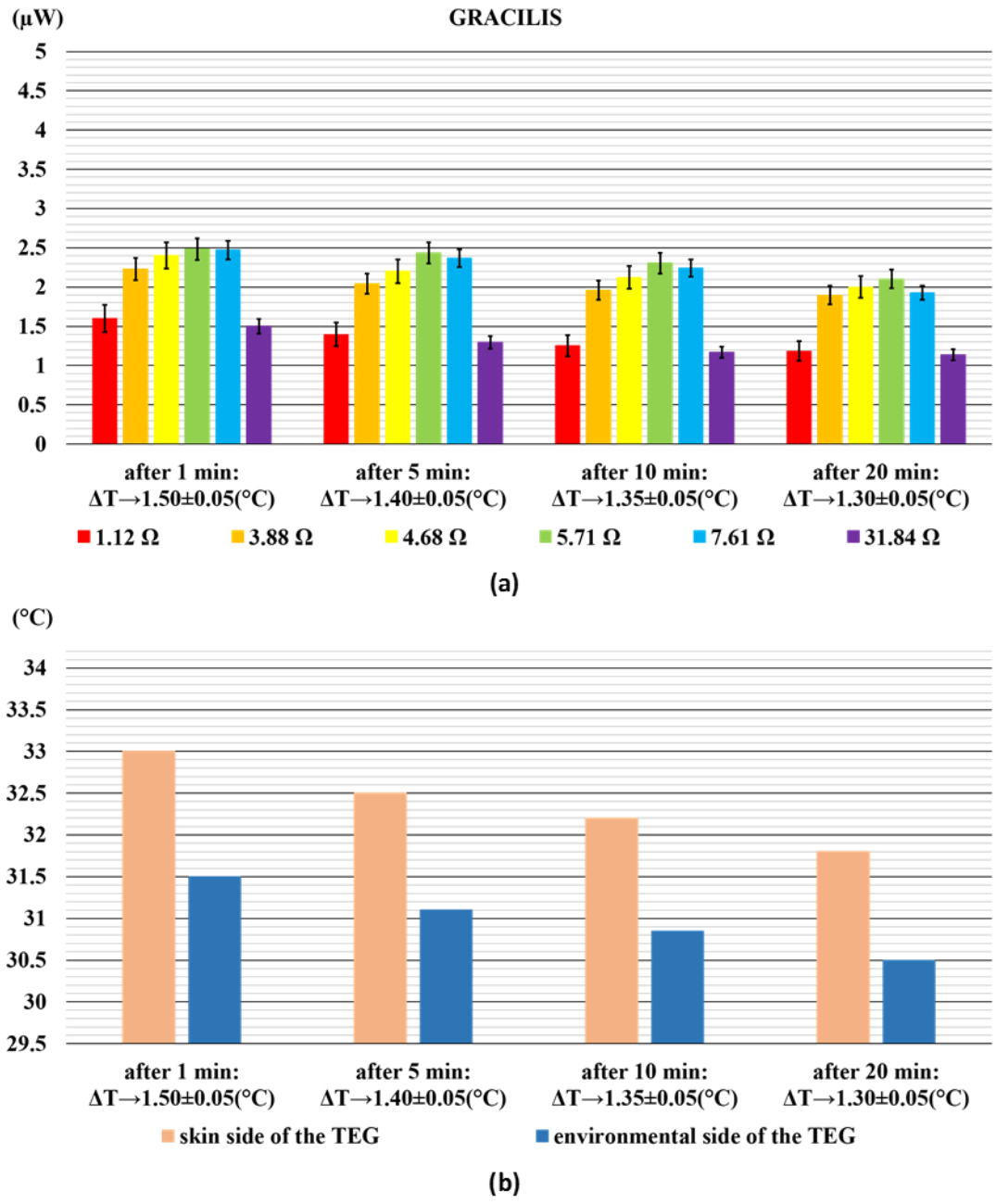

Figure 10C. *The power output generated by the TEG on the thigh, in correspondence to the flexor gracilis muscle* **(a)** *and the relative temperature difference* **(b)**.

In the diagram of ***Figure 10C*-(a)** the power output reached up to 2.6 μW after 1 minute of the performed test, and it decreased up to 2.1 μW at the end of the measurements. This variation

of about 0.5 µW depended on the decreasing of the temperature on both sides of the TEG. As it can be clearly seen in ***Figure 10C*-(b)**, it decreased from 1.50 °C to 1.30 °C.

***Figure 11C*-(a)** shows the power output generated by the TEG when it was on the calf, in correspondence to the gastrocnemius muscle, while ***Figure 11C*-(b)** shows the relative temperature difference during the experiment.

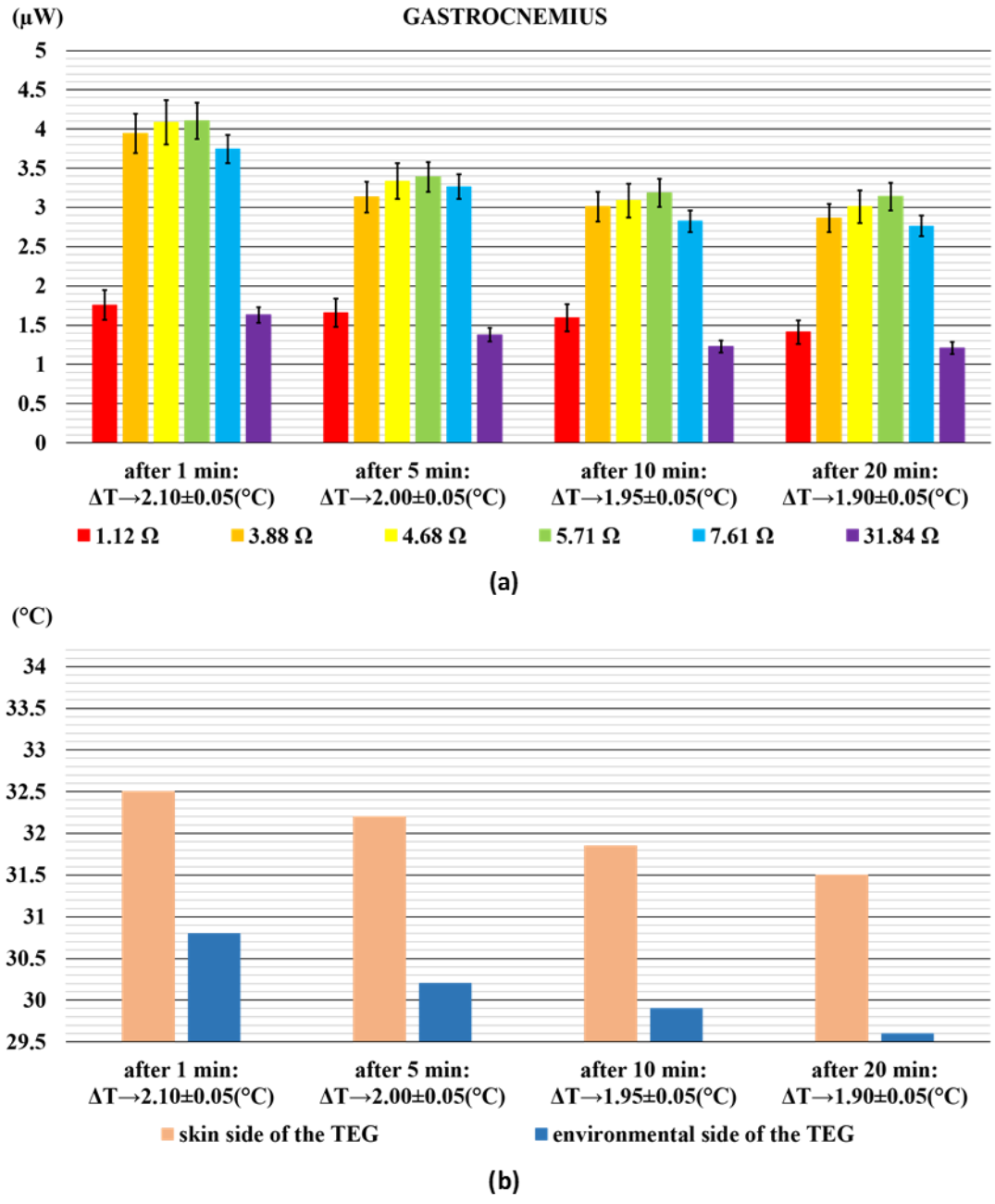

Figure 11C. *The power output generated by the TEG on the calf, in correspondence to the gastrocnemius muscle* **(a)** *and the relative temperature difference* **(b)**.

In the diagram of ***Figure 11C*-(a)** the power output reached up to 4.4 µW after 1 minute of the performed test, and it decreased up to 3.35 µW at the end of the measurements. This variation of about 1.05 µW depended on the decreasing of the temperature on both sides of the TEG. As it can be clearly seen in ***Figure 11C*-(b)**, it decreased from 2.10 °C to 1.90 °C.

For all the performed measurements, the power output graphs in ***Figure 8C–11C*** show a plateau corresponding to the middle values of the range of resistor loads. Particularly, 5.71 Ω is the value of the resistor load, which guarantees the largest power output, in the majority of the cases.

Therefore, in the second stage of the experiment, the activities such as sitting to rest, walking and jogging were performed by using in the measurement circuit, the resistor load of 5.71 Ω. ***Figure 12C*** shows the mean value plus the standard deviation value of the power generated by the TEG, during the repeated tests. The controlled room temperature was about 23 °C.

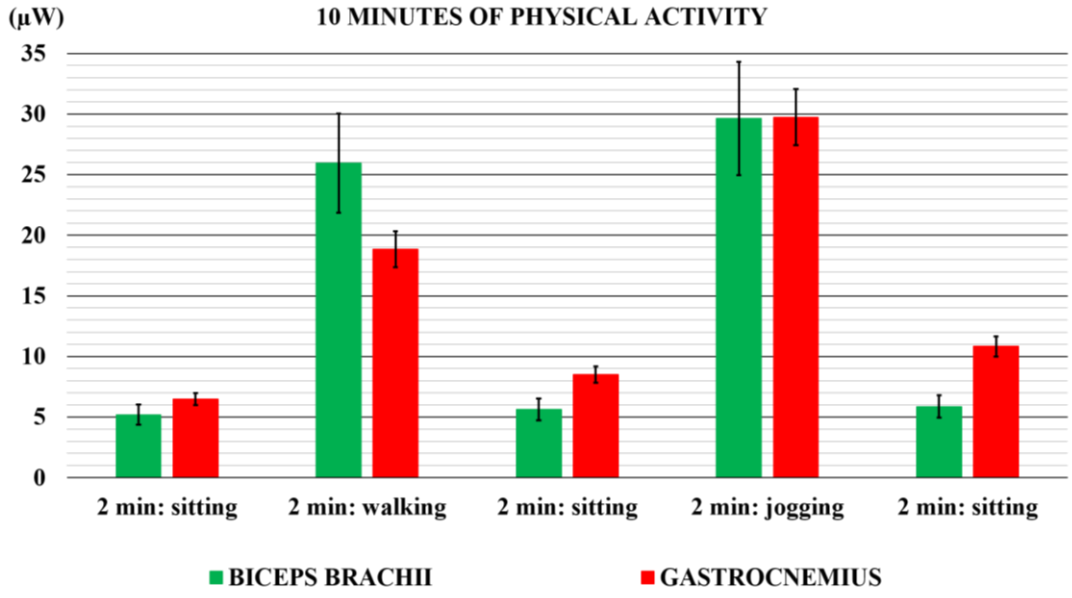

Figure 12C. *The mean values of the power output generated by the TEG on the calf, in correspondence to the gastrocnemius muscle* **(red bars)** *and on the arm anterior in correspondence to the biceps brachii muscle* **(green bars)**. *Four healthy male volunteers repeated the 10 minutes of physical activity for three times.*

The bar-diagram of ***Figure 12C*** shows the comparison of the power generated by the TEG placed in two different areas of the skin surface, by performing common daily activities. At first, it is important to denote that the value of the room temperature (23 °C) is 2°C lower than the room

temperature of the measurements in the first stage (25 °C) of the tests. Therefore, in ***Figure 12C*** the power values related to first two minutes of the sitting position (5.5 μW for the biceps brachii and 6.5 μW for the gastrocnemius) are quite higher than the values presented in ***Figure 11C*****-(a)** for the gastrocnemius (4 μW), and in ***Figure 8C*****-(a)** for the biceps brachii (4.5 μW). Again, the power values generated by TEG placed onto the arm during the three time periods of the sitting to rest activity are about the same, with a mean value of about 5.5 μW ± 0.3 μW. Conversely, the work of the gastrocnemius muscle during the walking and jogging activities allowed an increment of the power values for the performed sitting to rest activities, with a mean value of about 8.5 μW ± 2.0 μW. As regards, to the jogging activity, the power values for both the considered body parts are quite the same (30 μW), while as regards to the walking activity, the placement of TEG in correspondence to the biceps brachii muscle produced higher power values (25 μW) than the values generated by placing the TEG onto the gastrocnemius muscle (18 μW). In addition, it is easily to denote that the power generated by the arm is quite similar during the walking and jogging activities, by calculating a difference value of about at maximum 5 μW. Instead, the difference value between the power generated by the TEG on the calf during walking and jogging (12 μW) is much higher than the same difference recorded with the TEG on the arm. It is due to the muscular work of the gastrocnemius by performing these activities, which clearly increase in the jogging ones. Conversely, the work of the biceps brachii is about the same during walking and jogging and then, the power values of the two different activities are similar each other. Once again, as regards the walking and jogging activities, the values of the standard deviation for the measurements with the TEG placed onto the arm are much higher than those in which the TEG was attached to the calf. This result denotes that human beings move their arms more randomly than the movements of their limbs. In example, a man who swings his arms conspicuously, generates values of thermoelectric power much higher than the values produced by a man who almost does not moves his arms.

Finally, ***Figure 13C*** shows the sums of the mean values of the powers generated by the two considered body areas, the skin surface corresponding to the superficial muscles, such as the biceps brachii and the gastrocnemius, respectively.

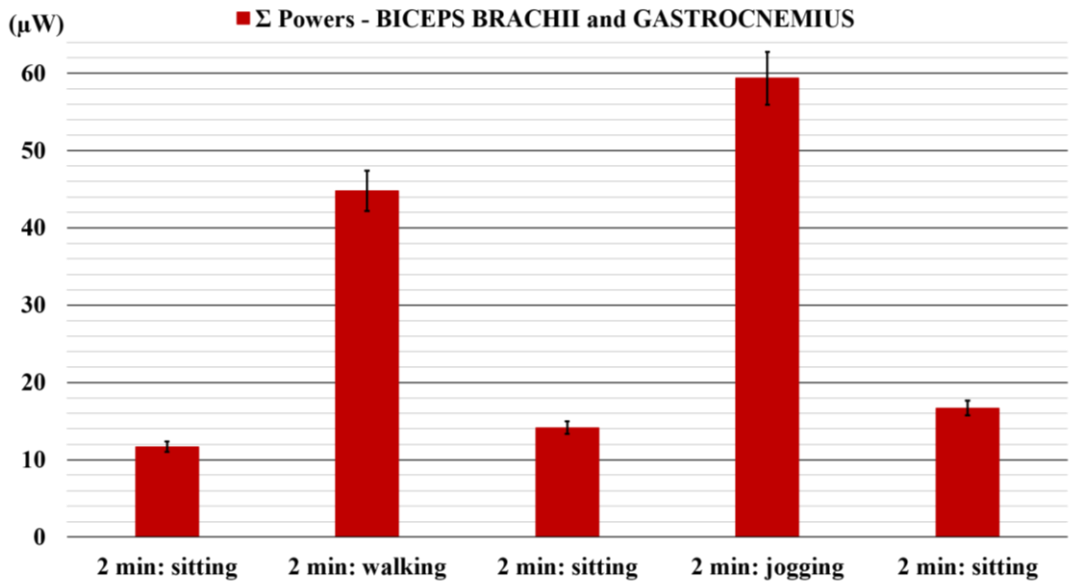

Figure 13C. *The sums of the mean values of the powers generated by the biceps brachii and the gastrocnemius muscles, by performing 10 minutes of physical activity.*

Table 3C summarizes the numerical values of ***Figure 13C***.

Table 3C. *Results of the sum of the power mean values measured on the skin areas related to biceps brachii and the gastrocnemius muscles*.

10 minutes of physical activity	Σ Powers – TES1-12704
First two minutes of sitting to rest	11.7 μW
Two minutes of walking	44.8 μW
Second two minutes of sitting to rest	14.1 μW
Two minutes of jogging	59.4 μW
Third two minutes of sitting to rest	16.7 μW

While examining the results in ***Table 3C***, the sums of the thermoelectric powers generated by the TES1-12704 module placed on the arm anterior and on the calf, are in the range of about 10 μW – 60 μW.

In addition, the value of power output generated by the TEG during the different activities can be used to recognize the performed physical activity. The sitting to rest activity produces power values much lower than the results of power output given by performing the two locomotion activities, i.e. walking and jogging. In a future study, it would be useful testing the behavior of the TEG to recognize and estimate the human daily activities.

HUMAN BODY MOTION: ENERGY HARVESTING AND DETECTION OF GAIT PHASES (D)

The results showed in this chapter are published in:

- ***Sensors, 16(4), 524*** *– Measurements of generated energy/electrical quantities from locomotion activities using piezoelectric wearable sensors for body motion energy harvesting.*
- ***Abstract Proceedings of the 3rd International Conference on Nanogenerators and Piezotronics*** *– Comparing PZT and PVDF as energy harvesters from human full body motion.*
- ***Proceedings of the 7th Biomedical Engineering Conference of Young Biomedical Engineers and Researchers*** *– Using PVDF films as flexible piezoelectric generators for biomechanical energy harvesting.*
- ***Proceedings of the IEEE-EMBS Conference on Biomedical Engineering and Science (IECBES-2016)*** *– Wearable PVDF transducer for biomechanical energy harvesting and gait cycle detection.*
- ***Abstract Proceedings of EMN Orlando Meeting 2016 on Electronic Textiles and Transparent Electrodes*** *– Micro/nanogenerators into clothes for harvesting biomechanical energy and sensing locomotion activities.*

4.1 BIOMECHANICAL CHARACTERISTICS OF THE HUMAN GAIT

The application field of biomechanical energy harvesting relies on the generation of renewable energy through the transduction and storing of the mechanical energy involved in human movements. Walking is the most common motion activity, and the analysis of the gait cycle allows the characterization of the biomechanical power involved in each phase of walking. The rigid-body model is the simplest way to represent the different parts of the body, and ***Figure 1D*** shows its main joints "j" and segments "s". Each joint is the junction point of at least two segments.

In the gait cycle analysis, the acquisition of kinetic and kinematics parameters is imperative to obtain quantitative information about the biomechanical work performed by body segments [138]**.** Kinetic parameters describe the study of forces and moments, which cause the motion; *i.e.* the joint reaction force acting on a segment "s" at the joint "j": $\mathrm{F}(\mathrm{j},\mathrm{s})$, and muscle reaction moments acting on a segment "s" at the joint "j": $\mathrm{M}(\mathrm{j},\mathrm{s})$. Instead, kinematic parameters describe the biomechanical movement without taking into account the forces that cause the movement: *i.e.* the linear velocity of the joint "j": $\mathrm{V}(\mathrm{j})$, and the angular velocity of the segment "s": $\omega(\mathrm{s})$.

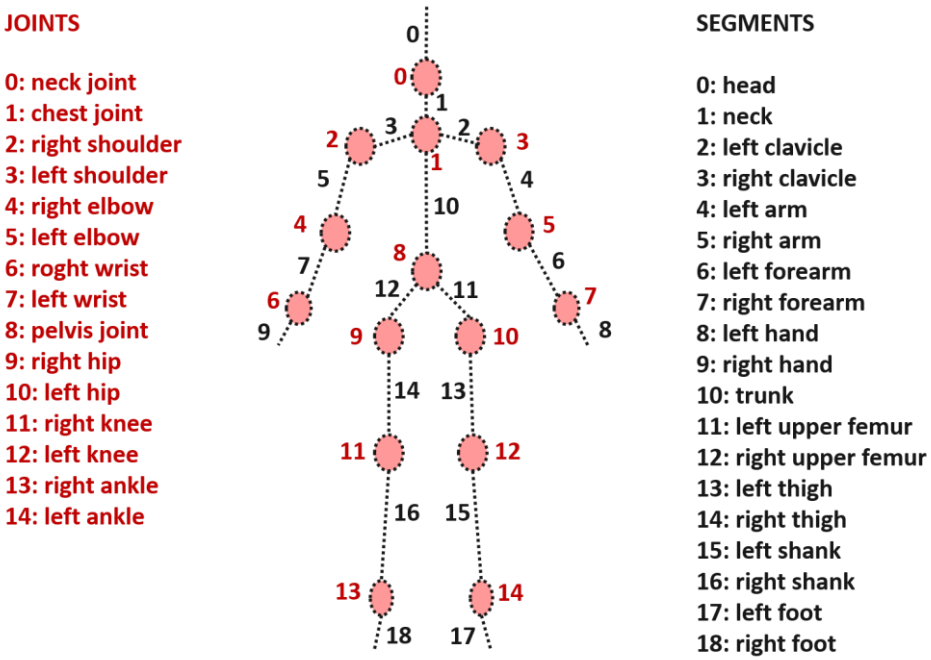

Figure 1D. *The rigid-body model for representing the main joints and segments of the human body.*

Thus, the total power delivered by a generic body segments "s", is the sum of the entire joint and muscle powers acting on such segment "s" at the joint "j", $(W_j(j,s)\,, W_m(j,s))$, as follows in *equation (1D)*:

$$(1D): \qquad W_t(s) = \sum_{j,m} [W_j(j,s) + W_m(j,s)] \quad ; \quad \begin{cases} W_j(j,s) = F(j,s)\, V(j) \\ W_m(j,s) = M(j,s)\, \omega(s) \end{cases}$$

As regards the *joint power* $W_j(j,s)$, the quantity $F(j,s)$ is the value of the reaction force for the segment "s" at the joint "j", and the quantity $V(j)$ is the absolute value of the velocity in the center point of the joint "j". A positive value for the *joint power*: $W_j(j,s) > 0$, indicates the rate of energy flow into the segment "s" at the joint "j", while a negative value for the *joint power*: $W_j(j,s) < 0$, shows the rate of the energy outflow from the segment "s". In *static condition*, it should be note that the value of the reaction force: $F(j,s_1)$, of a segment "s_1" has an equal and opposite value for an adjacent segment "s_2": $-F(j,s_1) = F(j,s_2)$, while the velocity values of both segments "s1" and "s2" are always the same: $V(j,s_1) = V(j,s_2)$. Thus, a flow of energy to the segment "s_1" implies an

equal outflow of energy from the segment "s_2". Therefore, the *joint powers* can show only rates of *energy transfer* between segments [139].

As regards the *muscle power* $W_m(j,s)$, the quantity $M(j,s)$ is the value of the joint moment acting on the segment "s" at the joint "j", and the quantity $\omega(s)$ is the angular velocity of the segment "s". A positive value for the *muscle power*: $W_m(j,s) > 0$, shows the rate of mechanical work done by the muscle "m" on the segment "s", while a negative value for the *muscle power*: $W_m(j,s) < 0$, represents a rate of mechanical work done by the segment "s" on the muscle "m". Contrary to the situation for the *joint powers*, the *muscle powers* of two adjacent segments "s_1" and "s_2", do not necessarily have the same angular velocity, so that the *muscle* can either *generate or absorb* biomechanical energy [139]. Thus, by studying the different phases of the gait cycle , it is possible to define how the body parts generate, absorb and transfer the biomechanical power.

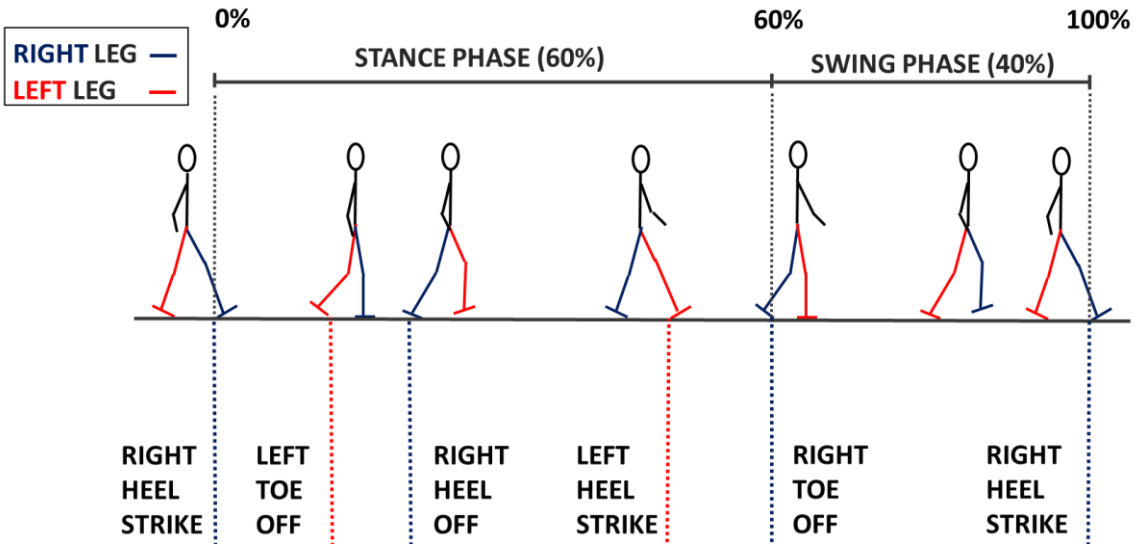

Figure 2D. *Picture for representing the human gait cycle.*

Figure 2D shows the human gait cycle. The stance phase and the swing phase divide the walk into two main periods, with 60% and 40% of the entire period, respectively [140]. ***Figure 2D*** assumes the start point of the stance phase when the right heel strikes the ground and it ends when the toe leaves the soil. Considering the same leg, the swing phase starts at the toe-off point and ends when the heel retouches the ground. Thus, a full cycle is completed.

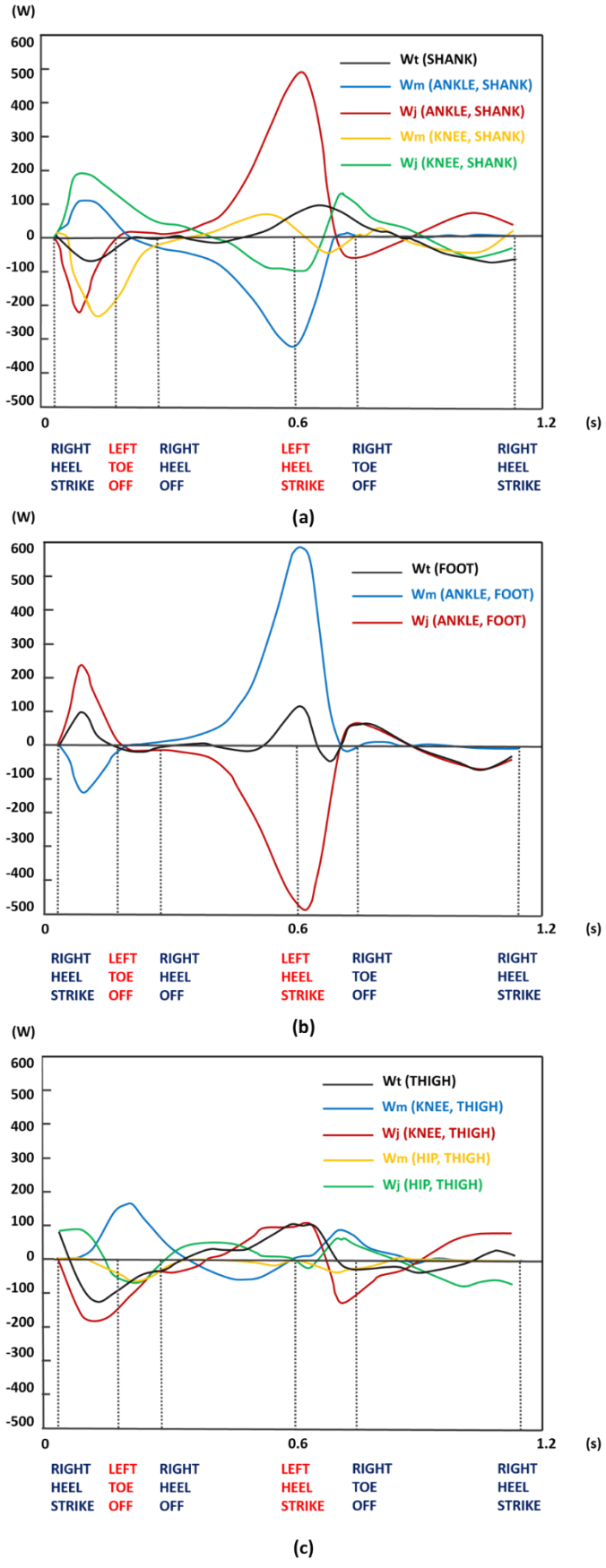

Figure 3D. *Patterns of joint, muscle and total powers of the shank* **(a)**, *foot* **(b)** *and thigh* **(c)** [139].

During walking, the total power delivered by the segments of the lower body are an order of magnitude higher than that originated from the upper anatomical parts; it is due to a rather small movement of the upper body during this activity [141], and negligible forces associated with it. The main segments of the lower body are the foot, the shank and the thigh, and the corresponding joints are the ankle, the knee and the hip. In gait analysis, regarding *power patterns*, the shank and foot segments tend to have similar power patterns. Conversely, the power pattern for the thigh segment appears distinct from those of shank and foot [139, 142].

Figure 3D shows the *power patterns* corresponding to the joint, muscle and total powers of the shank, foot and thigh during a gait cycle performed by a healthy man [139]. Generally, the ankle joint delivers the highest value of the power during the gait cycle.

4.2 TECHNIQUES FOR HARVESTING THE BIOMECHANICAL MOTION

Biomechanical energy harvesting means recovering energy from the body movement. It has been object of study by researchers from around the world for the past twenty years. Currently, the main problem is studying the feasibility of converting this kind of energy by using wearable and comfortable piezoelectric transducers.

Piezoelectric transducers convert mechanical deformations into electrical energy, as result of the direct piezoelectric effect, and conversely they transduce electrical energy to mechanical stresses, through the converse piezoelectric effect.

The following constitutive *equations (2D)* explain the relationship between the mechanical and electrical properties of piezoelectric materials:

$$(2D): \qquad \begin{bmatrix} \mathrm{S} \\ \mathrm{D} \end{bmatrix} = \begin{bmatrix} \mathrm{s_E} & d \\ \mathrm{d^T} & \varepsilon_\mathrm{S} \end{bmatrix} \begin{bmatrix} \mathrm{T} \\ \mathrm{E} \end{bmatrix} \quad \Leftrightarrow \quad \begin{cases} \mathrm{S} = \mathrm{s_E\,T} + \mathrm{d\,E} \\ \mathrm{D} = \mathrm{d^T\,T} + \varepsilon_\mathrm{S}\,\mathrm{E} \end{cases}$$

where S is the strain vector (6 x 1), T is the stress vector (6 x 1), D is the electric displacement vector (3 x 1), E is the electric field vector (3 x 1). Again, s_E is the stiffness matrix (6 x 6) evaluated at constant electric field, ε_{S} is the permittivity matrix (3 x 3) evaluated at constant stress, and d is the piezoelectric coefficients matrix (6 x 3).

In biomechanical energy harvesting applications, a stress field acts on to the piezoelectric transducer, generating an electric displacement in response. Therefore, the contribution of the external electric field is null, and the *equation (2D)* can be re-written as follows in *equation (2D-a)*:

$$(2D\text{-}a): \qquad \mathrm{D} = \mathrm{d}^{\mathrm{T}}\,\mathrm{T}$$

Generally, the piezoelectric transducer for the biomechanical energy harvesting application is a film (***Figure 4D***). Accordingly, and with reference to ***Figure 4D***, the electrical axis is always '3' (thickness axis: $\mathrm{t_p}$) and the mechanical axis can be either '1' (length axis: $\mathrm{l_p}$), '2' (width axis: $\mathrm{w_p}$) or '3' since the stress can be applied to any of these axes. Therefore, *equation (3D)* shows the complete form for the matrix treatment, as follows:

$$(3D): \qquad \begin{bmatrix} \mathrm{D_1} \\ \mathrm{D_2} \\ \mathrm{D_3} \end{bmatrix} = \begin{bmatrix} 0 & 0 & 0 & 0 & \mathrm{d_{15}} & 0 \\ 0 & 0 & 0 & \mathrm{d_{24}} & 0 & 0 \\ \mathrm{d_{31}} & \mathrm{d_{32}} & \mathrm{d_{33}} & 0 & 0 & 0 \end{bmatrix} \begin{bmatrix} \mathrm{T_1} \\ \mathrm{T_2} \\ \mathrm{T_3} \\ \mathrm{T_4} \\ \mathrm{T_5} \\ \mathrm{T_6} \end{bmatrix}$$

where the coefficients $\mathrm{d_{31}}$, $\mathrm{d_{32}}$, $\mathrm{d_{33}}$ relate the normal strain in the 1, 2 and 3 directions, respectively. Again, the coefficients $\mathrm{d_{15}}$ and $\mathrm{d_{24}}$ relate the shear strain in the 1-3 plane and the 2-3 plain, respectively. Note that the shear stress in the 1-2 plane: $\mathrm{T_6}$, is not capable of generating any electric response [34].

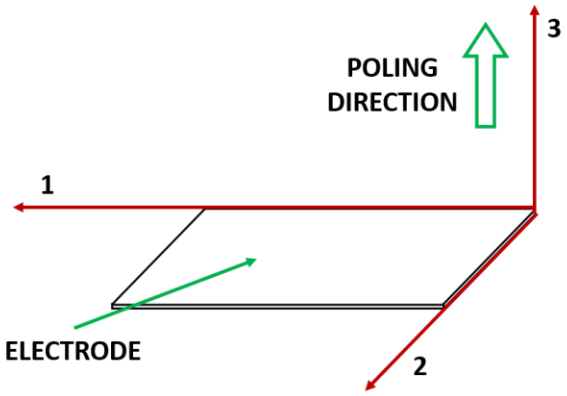

Figure 4D. *Numerical classification of axes of the thin film piezoelectric transducer: 1-length direction, 2-width direction and 3-thickness direction.*

By the value of the electrical displacement D, is possible calculate the generated charge by the following *equation (4D)*:

$$(4D): \qquad \mathrm{q} = \iint [\mathrm{D}_1 \quad \mathrm{D}_2 \quad \mathrm{D}_3] \begin{bmatrix} \mathrm{dA}_1 \\ \mathrm{dA}_2 \\ \mathrm{dA}_3 \end{bmatrix}$$

where dA_1, dA_2, dA_3 are the components of the electrode area in the 2-3, 1-3 and 1-2 planes, respectively. In *equation (4D)*, the generated charge q depends only on the component of the infinitesimal electrode area $\mathbf{dA}$, normal to the displacement $\mathbf{D}$.

Since a typical thin piezoelectric transducer can be treated as a parallel plate capacitor, whose capacitance is given by the following *equation (5D)*:

$$(5D): \qquad \mathrm{C_p} = \varepsilon_{\mathrm{S\_33}} \frac{\mathrm{w_p\, l_p}}{\mathrm{t_p}} = \varepsilon_{\mathrm{S\_33}} \frac{\mathrm{A}}{\mathrm{t_p}}$$

then, it is possible find the voltage generated across the electrodes of the piezoelectric transducer, as follows in *equation (6D)*:

$$(6D): \qquad \mathrm{V} = \frac{\mathrm{q}}{\mathrm{C_p}}$$

By analyzing the simplified equivalent electrical model of the piezoelectric transducer, it corresponds to a current generator with in parallel a capacitor. By putting a resistor load between the two ends of the piezoelectric element, is possible measure the power output generated by the

transducer, when an external mechanical stress occurs on its surfaces. ***Figure 5D*** shows the measurement circuit for the piezoelectric transducer.

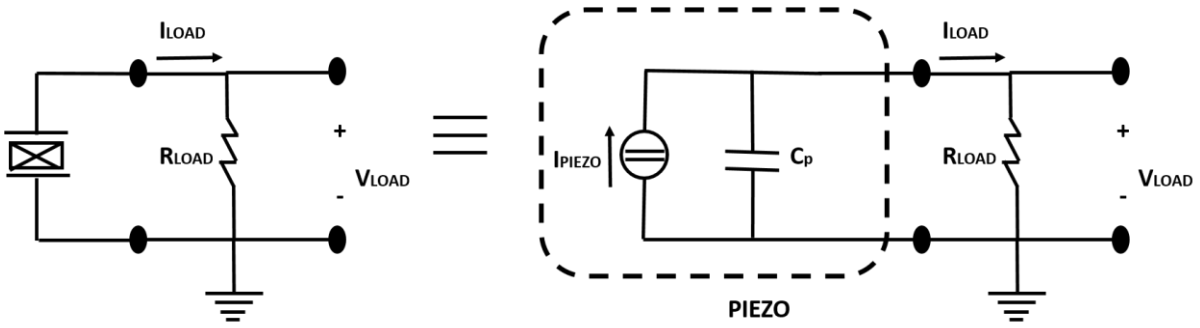

Figure 5D. *Circuit symbol of the piezoelectric transducer and its electrical measurement circuit.*

The following *equation (7D)* calculates the power output for the electrical circuit in ***Figure 5D*** [143]:

$$(7D): \qquad \mathrm{V_{LOAD}} = \mathrm{I_{LOAD}} \frac{\mathrm{R_{LOAD}}}{\sqrt{1 + \left(2\pi \mathrm{f C_p R_{LOAD}}\right)^2}} \quad \Leftrightarrow \quad \mathrm{P_{LOAD}} = \frac{\mathrm{V_{LOAD}^2}}{\mathrm{R_{LOAD}}}$$

In order to obtain the maximum value of the power output, the following *equation (8D)* should be satisfied:

$$(8D): \qquad \frac{\mathrm{dP_{LOAD}}}{\mathrm{dR_{LOAD}}} = \frac{\mathrm{d}\left(\frac{\mathrm{V_{LOAD}^2}}{\mathrm{R_{LOAD}}}\right)}{\mathrm{dR_{LOAD}}} = 0 \quad \Leftrightarrow \quad \mathrm{R_{LOAD}} = \frac{1}{2\pi \mathrm{f C_p}}$$

4.3 EXPERIMENTAL SECTION

4.3.1 PIEZOELECTRIC TRANSDUCERS CHOSEN

Piezoelectric transducers convert mechanical deformations into electrical energy, e.g., direct piezoelectric effect. Thanks to this property, the piezoelectric transducers can produce electrical energy from the movements of the body parts to which they adhere. The P-876.A12 transducer [144] and the LDT4-028k transducer [145] (***Figure 6D***) were chosen to analyze the power output of a biomechanical energy harvesting system, respectively based on soft PZT or on PVDF.

Figure 6D. *The P-876.A12 transducer* [144] *and the LDT4-028k transducer* [145].

The features of both P-876.A12 and LDT4-028k transducer are listed in ***Table 1D***.

Table 1D*. Properties of the P-876.A12 and the LDT4-028k transducers*.

Properties	**P-876.A12**	**LDT4-028k**
Density, ρ (g/cm^3)	7.8	1.8
Curié temperature, T_c (°C)	350	100
Relative permittivity, ε_r	1650–1750	12–13
Dielectric loss factor, σ	0.02	0.02
Coupling factor, k_t	0.47	0.14
Coupling factor, k_{31}	0.35	0.12
Coupling factor, k_{33}	0.69	-
Piezo charge coefficient, $\lvert d_{31} \rvert$ (10^{-12} C/N)	180	23
Piezo charge coefficient, $\lvert d_{33} \rvert$ (10^{-12} C/N)	400	33
Piezo voltage coefficient, $\lvert g_{31} \rvert$ (10^{-3} V m/N)	11.3	216
Piezo voltage coefficient, $\lvert g_{33} \rvert$ (10^{-3} V m/N)	25	330
Young's modulus, Y (10^9 N/m^2)	55.5	3.1
Minimum radius curvature, r_c (mm)	20	5
Active vol. dimensions (l × w × t) (mm)	(50 × 30 × 0.2)	(156 × 19 × 0.028)
Electrical capacitance, C (10^{-9} F)	90	12

4.3.2 HUMAN BODY MOVEMENTS CHOSEN

Seven body joints were chosen to harvest energy from body movements. These joints were chosen in order to measure the most common human body rotations: neck, shoulder, elbow, wrist, hip, knee and ankle are the joints around which the transducers were placed.

The angle values were manually measured by a goniometer, for each range of motion of the performed tests. These results were accepted on the basis of the results presented in the work of Reese and Bandy [146]. In ***Table 2D***, the body joint, joint movements, range of motion and the frequency motions are summarized.

Table 2D. *Body joints, body joint movements, range of motion* [146] *and frequency of tests.*

Body Joint	Joint Movement	Range of Motion (°)	Motion Frequency (Hz)
Neck	flexion-extension	58 ± 12	1.40± 0.10
Shoulder	adduction-abduction	140 ±9	1.10 ± 0.10
Elbow	flexion-extension	141 ± 8	1.25 ± 0.10
Wrist	flexion-extension	129 ± 14	1.90 ± 0.10
Hip	flexion-extension	138 ± 21	1.05 ± 0.10
Knee	flexion-extension	135 ± 11	1.15 ± 0.10
Ankle	plantar-dorsiflexion	66 ± 5	1.75 0.10

4.3.3 CHOICE on DAILY ACTIVITES

Five common locomotion activities were chosen to find out if the two piezoelectric transducers were efficient enough to harvest energy from the body movement in practice. The mentioned activities were walking, going down and up the stairs, jogging and running. The body joints chosen for the comparison of the two piezoelectric transducers were a subset of the aforementioned ones: elbow, ankle, knee, shoulder and hip. The flexion-extension movement of the wrist and neck were excluded from the measurements because these movements were deemed

as minor in terms of exerted forces during the chosen locomotion activities. In ***Table 3D***, the activities and their corresponding frequencies are summarized.

Table 3D. *Summary of the common activities and their frequencies*.

Common Activity	Frequency of the Activity (Hz)
Walking	1.15 ± 0.10
Walking downstairs	1.65 ± 0.10
Walking upstairs	1.05 ± 0.10
Jogging	1.60 ± 0.10
Running	2.10 ± 0.10

4.3.4 INTEGRATION INTO A SUIT: ELASTIC COTTON FABRICS

Piezoelectric transducers must be placed directly onto the skin to transduce the movements of the joints in the most appropriate way. Thus, a tight elastic cotton suit was made. Elastic cotton ensures proper adjacency to the body and comfort, and it is easy to clean.

The piezoelectric transducers were placed in the pockets of the suit, around each chosen joint. ***Figure 7D*** shows the blue suit with the green pockets, and a green belt which was used to capture ankle rotations.

Figure 7D. *The blue suit with the green pockets and a green belt*.

The positions of the transducers on the suit were chosen according to the value of their folding parameter, the minimum radius curvature. LDT4-028k is more flexible than P-876.A12, and

therefore, the former one was placed in the inner parts of the suit where the joints are at the maximum bending angle. The inner parts of the suit relate to the inner parts of the elbow, knee and shoulder. Conversely, P-876.A12 transducers were placed on the outer parts of those joints. The positions of transducers were the same for the measurements of the wrist, neck, ankle and hip joints. ***Table 4D*** shows the reference positions for the transducers referring to the numbers in ***Figure 7D***.

Table 4D. *Positions of the transducers on the suit and on the belt*.

Numbers in Figure 2	Joint, Transducer	Reference Position for the Measurements
1	Wrist, P-876.A12	Top of wrist
2	Wrist, LDT4-028k	Top of wrist
3	Elbow, P-876.A12	Outer elbow
4	Elbow, LDT4-028k	Inner elbow
5	Neck, P-876.A12	Back of the neck
6	Neck, LDT4-028k	Back of the neck
7	Knee, P-876.A12	Outer knee
8	Knee, LDT4-028k	Inner knee
9	Hip, P-876.A12	Front hip
10	Hip, LDT4-028k	Front hip
11	Shoulder, P-876.A12	Outer shoulder
12	Shoulder, LDT4-028k	Inner shoulder
13	Ankle, P-876.A12	The ankle plantar
14	Ankle, LDT4-028k	The ankle plantar

4.3.5 HUMAN BODY ENERGY HARVESTING – EXPERIMENTS AND DATA DISCUSSION

To find out the voltage output, the measurement circuit shown in ***Figure 5D*** was used, and the values of the voltage output were measured and acquired by the NI USB-6210 data acquisition system (DAQ), National Instruments. A voltage divider circuit was used as the input stage of the NI USB-6210 DAQ in order to avoid the problem of saturation given by the range of voltage values at the input stage of the DAQ. The voltage output for the circuit in ***Figure 5D*** is given by the *equation (7D)* shown in the above section, so as the formula for the power output.

In order to optimize the power output, the ranges of fixed values of the resistors were carefully chosen based on the transducers datasheets [147, 148] and on the motion frequency of the joint movements. Therefore, ***Table 5D*** shows the range of values of the resistor loads.

To ensure that the P-876.A12 transducer could be bent properly, perfectly following the whole movement of the joints, it was necessary to place an extra elastic band over the suit, to make the transducers adhere to the body part during movement. Conversely, the LDT4-028k transducers did not need any additional support to secure their placement, due to their higher flexibility and ability to follow the joint movements.

To obtain the root mean square values of the voltages, currents and powers, the measured values of the peak-to-peak voltage output were used in the following *equation (9D)*.

$$(9D): \qquad \mathrm{V_{rms}} = \frac{\mathrm{V_{LOAD}}}{2\sqrt{2}} \Rightarrow \mathrm{I_{rms}} = \frac{\mathrm{V_{rms}}}{\mathrm{R_{LOAD}}} \Rightarrow \mathrm{P_{rms}} = \mathrm{V_{rms}I_{rms}}$$

Table 5D. *The chosen fixed values of the resistors*.

R_{LOAD} → P-876.A12 Transducer	R_{LOAD} → LDT4-028k Transducer
0.075 MΩ	1.865 MΩ
0.220 MΩ	3.715 MΩ
0.440 MΩ	5.745 MΩ
0.610 MΩ	7.100 MΩ
0.830 MΩ	8.530 MΩ
0.900 MΩ	10.545 MΩ
1.180 MΩ	13.180 MΩ
1.400 MΩ	14.930 MΩ
1.850 MΩ	17.215 MΩ
2.400 MΩ	18.775 MΩ
3.600 MΩ	22.340 MΩ
5.850 MΩ	25.175 MΩ

Equation (9D) was used to find the RMS values from each performed movement repetition, shown in ***Table 2D***. In the case of these movements, the nature of the angular movements could be roughly approximated to *equation (9D)*, even if it deviates from a pure sinusoidal tone, as is shown in ***Figure 8D***.

Three healthy male volunteers (age: 34 ± 5 year; body weight: 76 ± 4 kg; height: 175 ± 5 cm) were recruited to perform the joint movements listed in ***Table 2D***. Each joint movement was repeated five times, and the measuring time for each test was around ten seconds.

Figure 9D shows output RMS power values coming from the body joints for each value of the resistive load. Both transducers produce a signal output proportional to the folding movement and frequency of the performed test.

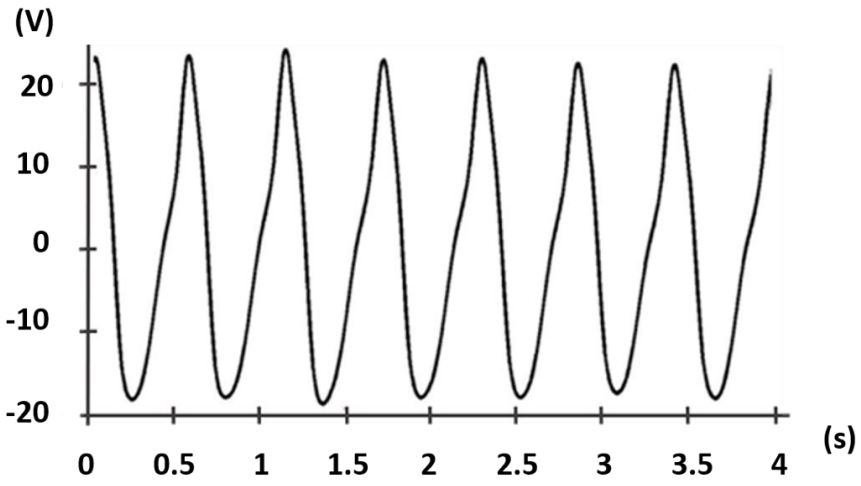

Figure 8D. *Sample of the voltage output measured by using the LDT4-028k transducer placed on the elbow joint for the movement of flexion-extension. The calculated RMS value corresponds to 13.78 V, slightly less than the value that could be obtained if Equation (6), for sinusoidal waves, had been applied (14.62 V).*

To obtain the maximum value of the power output, the most important parameter is the proper positioning of the transducer on the suit close to the skin, so that it can be bent as much as possible. The inherent different nature of the transducers makes it difficult to use the same exact location for both sensors, since the rigidity of the P-876.A12 transducer makes it necessary to provide the user with a sustaining structure and a different placement as compared to the LDT4-028k transducer. This consideration makes it impossible to directly compare the power output of transducers, but since the focus of the work is on the applicability of the transducers in real-life conditions, the comparison between transducers needs to include the positioning choice, as well.

In the P-876.A12 transducer diagram (***Figure 9D*-(a)**), the power outputs for the elbow joint are higher than those obtained for the other joints. In the graph of the LDT4-028k transducer (***Figure 9D*-(b)**), the highest power output values are those related to wrist, knee and hip joints. For both transducers, the values of the power output increase with the increase of R_{LOAD} to reach a maximum value, and then, they gradually decrease. Comparing the two graphs in ***Figure 9D***, the maximum values of the power output for P-876.A12 on the elbow (49.1 μW), ankle (4.94 μW), wrist (22.2 μW)

and neck (7.68 µW) joints are higher than those obtained by LDT4-028k on the same joints. Conversely, the maximum values of the power output for LDT4-028k on the shoulder (12.3 µW), knee (15.9 µW) and hip (15.0 µW) joints are higher than those appearing for P-876.A12 placed on the same joints.

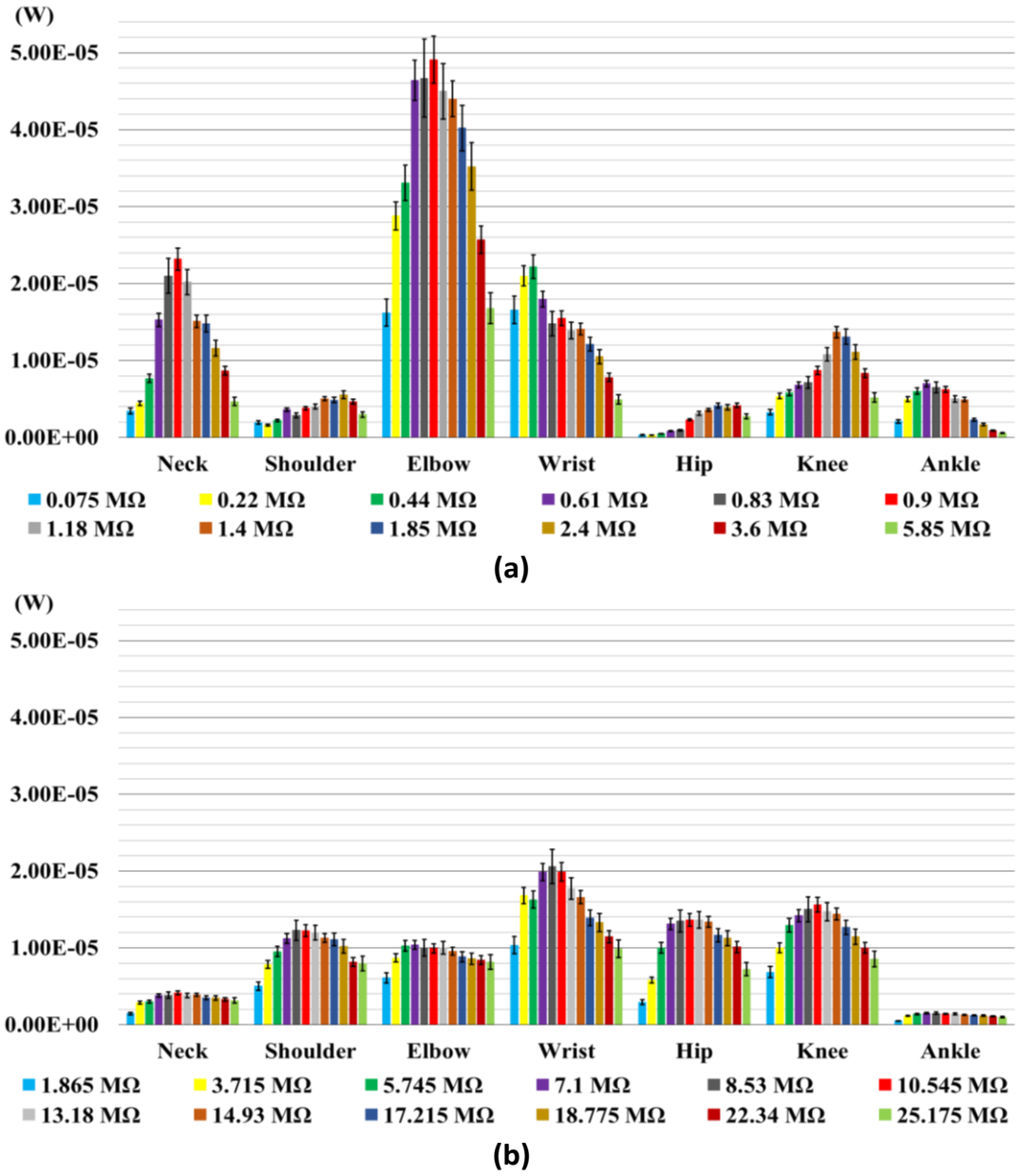

Figure 9D. *The calculated mean values of the power output for each value of the load resistor. Error bars represent standard deviations*. **(a)** *P-876.A12*; **(b)** *LDT4-028k*.

After these firsts measurements, five common activities were chosen to test the two piezoelectric transducers. The chosen common activities were walking, walking down and up stairs, jogging and running, and the chosen joints for the tests were the shoulder, elbow, hip, knee and ankle. For each activity, the values of the voltage were measured and acquired by the NI USB-6210 DAQ, National Instruments, while the values of the current and the power, based on a fixed value of the resistive load, were calculated using the MATLAB software. A voltage divider circuit was used as the input stage of the NI USB-6210 DAQ to avoid saturation given by the range of voltage values at the input stage of the DAQ. The fixed values of the resistive load, based on the previous measurements (***Figure 9D***), were carefully chosen for each joint, and they are shown in ***Table 6D***. These values were obtained through interpolation and approximation of the discrete values tested in the first experimentation.

Table 6D. *The fixed values of the resistors for each joint*.

Joint	**R_{load} → P-876.A12**	**R_{load} → LDT4-028k**
Shoulder	2.000 MΩ	8.880 MΩ
Elbow	0.952 MΩ	7.880 MΩ
Hip	2.000 MΩ	10.565 MΩ
Knee	1.430 MΩ	10.565 MΩ
Ankle	0.952 MΩ	7.080 MΩ

The tests were repeated for each reported resistance value, and thus, the values of the power output were obtained in statistical terms as average values across multiple repetitions, to take into account the inherent variability of having different participant samples repeating the mentioned activities.

Three healthy male volunteers (age: 34 ± 5 year; body weight: 76 ± 4 kg; height: 175 ± 5 cm) were recruited to perform the activities listed in ***Table 3D***. Each task was repeated four times. The

measuring time of walking and walking down and upstairs was one minute for each test, while the measuring time of the jogging activity was twenty seconds and for the running activity eight seconds.

Also for these tests, the inherent different nature of the transducers makes it difficult to use the same exact location for both sensors, since the rigidity of the P-876.A12 transducer makes it necessary to provide the user with a sustaining structure and a different placement as compared to the LDT4-028k transducer.

Figure 10D shows the measurements of the RMS power output values of the body joints, for each performed activity. Locomotion activities, such as walking and walking up stairs, produce the lowest values of the power output for both transducers, while running produces the highest values for both of them, followed by power output values of jogging and walking down stairs.

As can be clearly seen in ***Figure 10D*-(a)**, walking, walking up stairs and walking down stairs, for P-876.A12, led to very similar power output. Out of these three activities, the knee joint produces the highest values of power output (2.21 μW) followed by the ankle (0.54 μW), elbow (0.41 μW), shoulder (0.31 μW) and hip (0.20 μW) joints. As for the jogging activity, the knee joint produces the highest value of power output (5.98 μW) followed by the shoulder (2.24 μW), ankle (1.45 μW), elbow (0.60 μW) and hip (0.31 μW) joints. As for running, the knee joint produces the highest value of the power output (23.70 μW) followed by hip (9.37 μW), elbow (8.16 μW), shoulder (3.12 μW) and ankle (1.65 μW) joints.

Similar considerations apply to the LDT4-028k transducer (***Figure 10D*-(b)**), though with lower absolute values. In all activities, except running and jogging, the knee joint produces the highest value of power output (1.90 μW) followed by the hip (0.95 μW), ankle (0.67 μW), elbow (0.25 μW) and shoulder (0.21 μW) joints. As for jogging, the knee joint produces the highest value of power output (3.71 μW) followed by the ankle (2.88 μW), hip (2.43 μW), elbow (1.86 μW) and

shoulder (4.46 µW) joints. As for running, the knee joint produces the highest value of power output (8.83 µW) followed by the shoulder (5.16 µW), ankle (5.13 µW), elbow (4.83 µW) and hip (4.46 µW) joints.

Table 7D breaks down the comparison between P-876.A12 (PZT) and LDT4-028k (PDVF) considering all of the locomotion activities and all of the joints, highlighting which transducer performed best for each activity and joint.

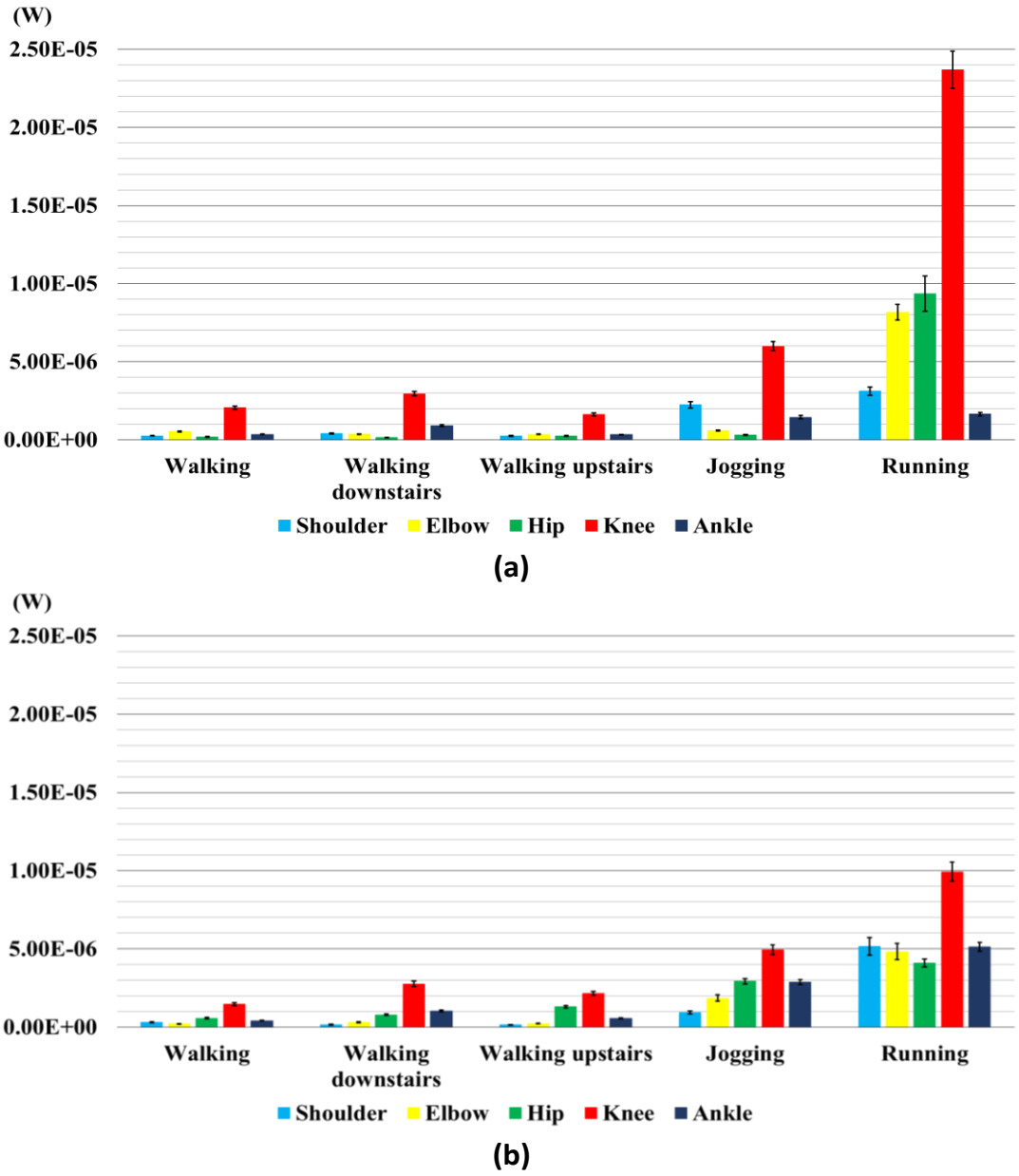

Figure 10D. *Comparison of the calculated grand mean values of power output on each joint for each activity. Error bars represent standard deviations.* **(a)** *P-876.A12;* **(b)** *LDT4-028k.*

Table 7D. *Comparison between the two transducers based on the five locomotion activities. PZT, lead zirconate titanate.*

Joint	Walking		Walking down Stairs		Walking up Stairs		Jogging		Running	
	PZT	**PVDF**	**PZT**	**PVDF**	**PZT**	**PVDF**	**PZT**	**PVDF**	**PZT**	**PVDF**
Shoulder	=	=	+	-	=	=	+	-	-	+
Elbow	+	-	=	=	=	=	-	+	+	-
Hip	-	+	-	+	-	+	-	+	+	-
Knee	+	-	=	=	=	=	+	-	+	-
Ankle	=	=	=	=	=	=	-	+	-	+

Differences in power harvesting between transducers: the symbol "+" represents the transducer with the highest value of power output, and conversely, the symbol "-" represents the transducer with the lowest value of power output. The symbol "=" represents transducers of very similar values of power output.

During walking, the values of the power output measured at each joint were very similar for both transducers: elbow (+0.31 μW) and knee (+0.47 μW) joints provide better results with P-876.A12, while the hip joint (+0.66 μW) is better with LDT4-028k.

Similar considerations apply to the case of walking down stairs, with slightly better results on the shoulder joint (+0.26 μW) for P-876.A12 and better on the hip joint (+0.52 μW) for LDT4-028k.

In the case of walking up stairs, LDT4-028k provides clearly better results than P-876.A12 at the hip joint (+1.08 μW). As for the jogging activity, P-876.A12 provides better results both at the shoulder (+1.30 μW) and at the knee (+2.27 μW) joints, while LDT4-028k resulted in being better for the elbow (+1.26 μW), hip (+2.12 μW) and ankle (+1.43 μW) joints. Finally, in the case of running, P-876.A12 performed better than LDT4-028k at the elbow (+3.33 μW), hip (+4.91 μW) and knee (+14.87 μW) joints, while the opposite applies to the shoulder (−2.04 μW) and ankle (−3.48 μW) joints.

The graph in ***Figure 11D*** shows the results of the overall comparison between the transducers, by considering the sum of the power output values measured at each joint for each locomotion activity. From the overall comparison, transducers are similar in terms of power generation for both walking and walking down stairs; when walking upstairs and jogging, LDT4-028k is more efficient than P-876.A12. Finally, during running, even if both transducers are appropriate for use as energy harvesters, the PZT transducer performed better than PVDF. The numerical values are summarized in ***Table 8D***.

Table 9D breaks down the power generated by the ones that come from the upper body joints and the ones coming from the lower limb joints. The power contribution from the upper body joints is almost negligible for the three walking activities, while it can be considered as a significant source of power generation for both jogging and running.

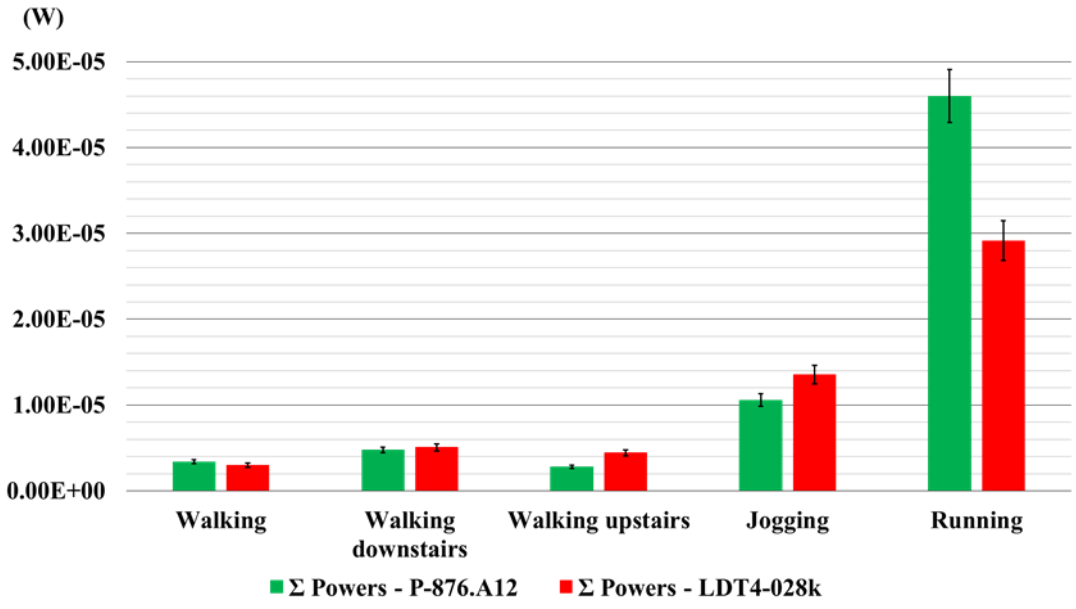

Figure 11D. *The sums of the mean values of the calculated power output on each joint for the activity performed. Error bars represent the standard deviation.*

Table 8D. *Results of the sum of the power grand mean values measured at all of the joints for each activity.*

Activity	∑ Power, P-876.A12	∑ Power, LDT4-028k
Walking	3.39 µW	3.38 µW
Walking downstairs	4.79 µW	4.38 µW
Walking upstairs	2.81 µW	4.18 µW
Jogging	10.60 µW	11.81 µW
Running	46.00 µW	28.41 µW

Table 9D. *Results shown in* ***Table 8D*** *divided by joint position: upper body and lower body.*

Activity	∑ Power, P-876.A12		∑ Power, LDT4-028k	
	Upper Body	Lower Body	Upper Body	Lower Body
Walking	0.78 µW	2.61 µW	0.52 µW	2.86 µW
Walking downstairs	0.78 µW	4.01 µW	0.47 µW	3.91 µW
Walking upstairs	0.60 µW	2.21 µW	0.39 µW	3.79 µW
Jogging	2.84 µW	7.74 µW	2.81 µW	9.00 µW
Running	11.28 µW	34.72 µW	9.99 µW	18.42 µW

As it can be clearly seen from the proposed results, the power output measured at each joint is sufficient to consider both transducer suitable to be used as energy harvesters for applications of biomechanical energy harvesting.

When comparing the performed tests, it resulted that soft PZT technology is more efficient than the PVDF in terms of generated power output; however, PVDF technology is more comfortable in terms of user wearability, which is the most important parameter to consider in this kind of systems.

4.3.6 DETECTION OF GAIT PHASES – EXPERIMENTS AND DATA DISCUSSION

This section shows a preliminary study about the use feasibility of the LDT4-028k PVDF biomechanical harvester as an active sensor, able to classify the two main phases of the human gait, the stance and the swing phases, respectively. The PVDF sensor was placed in close contact with the skin, in order to obtain a wearable, flexible and non-invasive system for the users.

The standard criterion to detect the gait events through an ambulatory system is based on the use of footswitches but, in recent times, many researchers studied the spatio-temporal parameters of walking by using gyroscopes. Aminian *et al*. [149] described a system for the estimation of gait events by using miniature gyroscopes. Their method was validated based on results achieved by footswitches. Formento *et al*. [150] proposed gait events detection using a rate gyroscope and Rueterbories *et al*. [138] reviewed the main techniques to analyze human gait by using multiple inertial sensors.

In this preliminary test, the pattern of the output signal from the LDT4-028k during the walking activity, was compared with the pattern of the output signal from a gyroscope, the Shimmer3 IMU system [151], to study the feasibility of the LDT4-028k transducer for the classification of the phases of human gait.

Figure 12D shows the position of the transducer and the gyroscope on the knee left leg. The gyroscope was placed at the end level of the PVDF element.

A healthy male volunteer (age: 29 years; body weight: 72 kg; height: 170 cm) was recruited to perform the test. The volunteer walked fifty meters in a long straight direction for six times, and the data were simultaneously acquired from both systems.

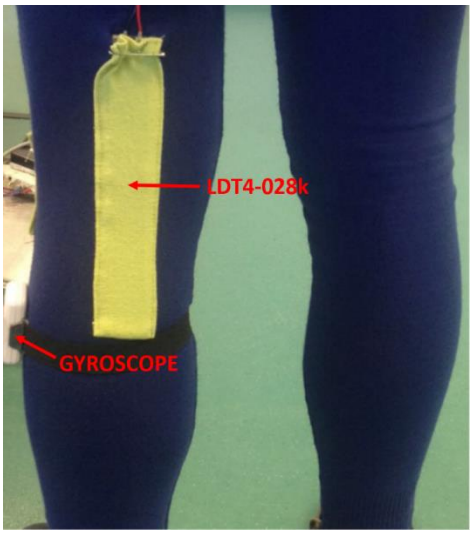

Figure 12D. *Position of the LDT4-028k transducer and the Shimmer3 IMU. Location at the back of the knee left leg*.

In order to efficiently compare the two patterns, we elaborated the output signals from both the transducer and the gyroscope through the following sequence: at first by the synchronization of the two output signals; then, with a 0.05 Hz high pass filtering of both signals; finally normalizing values in the range 0 to 1.

Therefore, ***Figure 13D*** shows the comparison between the transducer and gyroscope signals. The six graphs are listed based on the value of the walking frequency, from 0.861 to 0.985 Hz. The bold red line represents the mean value of the PVDF transducer track; the bold blue line is the mean value of the gyroscope track. The blue and red areas around the bold lines represent the standard deviations. The green dashed line is the toe-off point where the swing phase starts; the yellow dashed line is the heel strike point, i.e. the starting point of the stance phase. Finally, the violet double arrow denotes the period of the swing phase (in %), and the brown double arrow represents the stance phase period (in %).

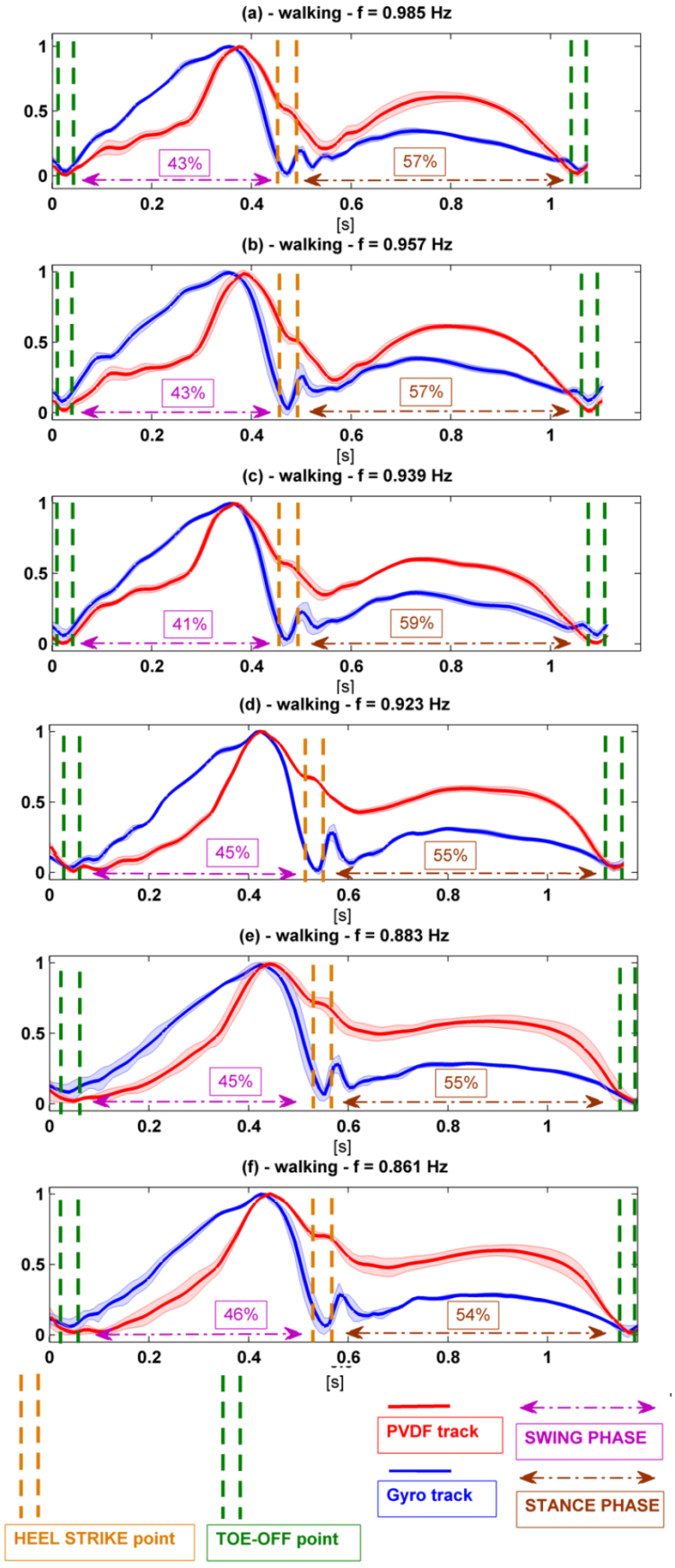

Figure 13D. *Comparison between the transducer (LDT4-028k) and gyroscope (Shimmer3 IMU) walking output signals for six different gait speeds.*

In addition, ***Figure 14D*** details the comparison between the walking output signals of the transducer and gyroscope, which concerns the feasibility of using the LDT4-028k transducer as biomechanical sensor for gait analysis. The red line is the track of the PVDF film and represents the displacement of the transducer during walking. The blue line is the track of the gyroscope and describes the angular velocity of the shank with respect to the sagittal plane. The two signals represent different variables (in rough terms, while the gyroscope measures an angular rate, the PVDF estimates an amount of joint rotation); therefore, they cannot be compared in terms of amplitude parameters. Nevertheless, we want to compare their signal patterns, in terms of waveform.

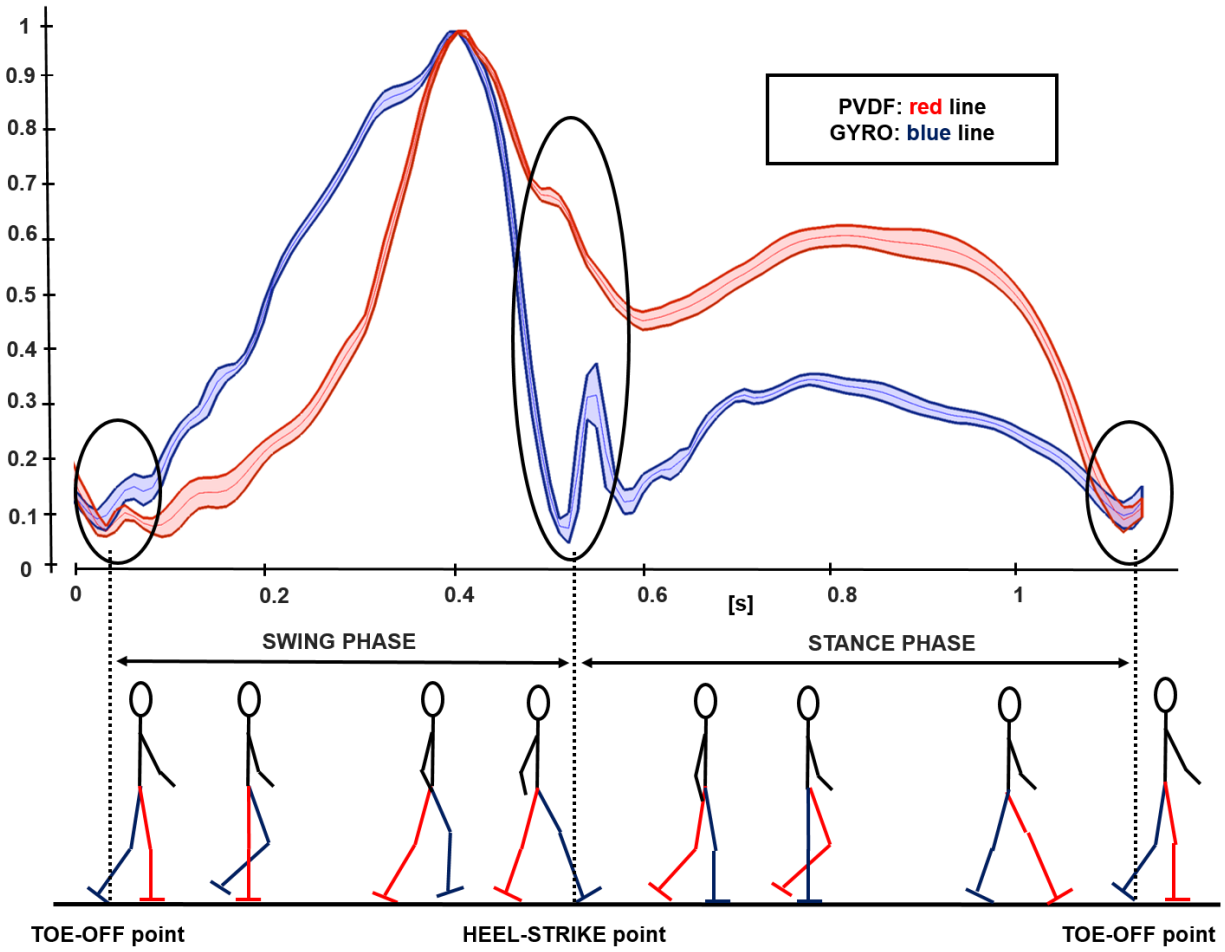

Figure 14D. *Detail of one comparison between the transducer (LDT4-028k) and the gyroscope (Shimmer3 IMU) walking output signals (see* ***Figure 13D*** *panel d).*

In ***Figure 14D***, the toe-off and the heel-strike points are highlighted with a black oval circle to evaluate the proposed result, in light of the study by Aminian *et al*. [149]. These two points are the starting points of the swing and stance phases of the foot during the gait cycle. As for the output track of the LDT4-028k transducer, the toe-off time instant that may be estimated from the PVDF almost fully overlaps with the one calculated from the gyroscope output signal. Instead, at the start of the stance phase, the track of the LDT4-028k presents a variation in the slope of the curve, almost to form a saddle point. This variation is limited but shows that the PVDF transducer on the knee joint may be used to allow distinguishing between the two phases of gait. Indeed, the PVDF transducer and the gyroscope identify the two phases of gait with an average time difference of about 15 ms. Again, in ***Figure 13D***, we report the percentages of the time period of the two phases, which are in line with the common results of the ambulatory methods for detecting the phases of gait cycle: 40% for the swing phase and 60 % for the stance phase [140].

GENERAL CONCLUSIONS (E)

The aim of this thesis was to study the application field about the energy harvesting from the human body. Particularly, the human beings generate energy by the biomechanical motion performed during the daily activities and continuously produce thermal energy by the dissipation of the body heat in the environment. This field of research is very recent, since the first theoretical work dates back to the '90s [20].

In the chapter of the literature review, the first two sections point out the macro-size transducers for harvesting the biomechanical and thermal energy generated by the human body. Specifically, the piezoelectric and Seebeck effects are the working principles of the biomechanical and thermal transducers, respectively.

As regards the biomechanical energy harvesting, the section begins explaining the choice of the piezoelectric transducers as the best harvesters for the aim of this thesis. Then, a short review about the classification of the piezoelectric harvesters based on their placement on the body surface is given. The optimum biomechanical energy harvester should be a flexible thin film element to allow the everyday life activities, without feeling discomfort to the wearer.

As regards the energy harvesting from the human heat, the proposed section starts by showing the history of the thermoelectric generator (TEG) for the applications of recovering the energy on the body. Firstly, the TEG were integrated into wearables, such as wristwatches or devices for monitoring the bioelectrical signals; then, the researchers developed TEG directly onto garments, such as shirts, jackets and also caps. To the author knowledge, there is a notable lack of studies targeting the placement of TEGs on the lower limbs. Naturally, the skin temperature of the legs is lower than the skin temperature of the arms, but by performing physical activities, such as walking or jogging, leads to an increase of the temperature in correspondence of the superficial

muscles of the legs. Therefore, the development of smart socks with integrated TEGs it would be a good design choice for harvesting the energy on the human body.

In the third section of the literature review chapter, the main aim was to show the newest technology for harvesting the mechanical and thermal energies. These new technologies rely on the use of nanogenerators (NGs). The NGs can be bent, twisted and stretched but retain their original electronic and structural properties. Up to now, the piezoelectric, triboelectric and thermoelectric effects are the most known operating principles for designing NGs. Piezoelectric and triboelectric NGs for harvesting the mechanical energy while thermoelectric NGs for recovering the thermal energy.

As regards the piezoelectric NGs, the most used materials are the nanowires of ZnO, but also the PZT, the $BaTiO_3$ and the PVDF are largely used for developing NGs. Particularly, the world countries most involved in developing of piezoelectric NGs are the USA, China and South Korea.

The triboelectric NGs rely on the friction mechanism between two materials with different value of electronegativity. For this reason, both the metals that the plastics can be used as triboelectric surfaces, but also the glass or even the human skin can be employed to develop triboelectric NGs. There are four fundamental modes for designing TENGs: the *vertical contact-separation mode*; the *in-plane sliding mode*; the *single-electrode mode* and the *free-standing triboelectric-layer mode*. For the purpose of the human body energy harvesting, the first one is the most studied in literature since the vertical contact and separation between two surfaces can be well represented by slamming the heel to the ground during walking. As regards the second and the fourth modes in the scientific literature, there are not relevant examples of NGs for harvesting the energy from the human body. Instead, the third one is the most promising mode to design NGs for the applications of the biomechanical energy harvesting. It is due to the use of the human skin as one of the two triboelectric surfaces. By comparing the piezoelectric and triboelectric NGs, the latter

ones produce the highest values of power output but the former ones are most reliable since they are studied by more time.

As regards the thermoelectric NGs, there are few examples in the scientific literature. It is due to the lower values of the power output compared to the values generated by the piezoelectric and triboelectric NGs.

In order to incorporate the NGs into clothes, the simplest way is to develop fibers able to harvest the energy. Particularly, the movements of the fibers within the garments allow the mechanical energy harvesting; then, in the scientific literature there are several examples of piezoelectric and triboelectric fibers for harvesting this kind of energy. Therefore, the fibers for harvesting the energy are the best choice for developing smart garments that can be worn at any time of the day.

Finally, in the last part of the literature review chapter, the discussion about the textile devices for sensing shows the potentiality of such technology for the health's monitoring of people in the least invasive way as possible.

In the experimental sections of the proposed thesis, many tests were done in order to understand which are the values of the power that can be harvested in daily life activities.

At first, the human heat and the environmental aspects were studied to understand the real possibility to recover the thermal energy on the surface of the body. Therefore, the TES1-12704 module was sewn in a band and two body locations were chosen to perform the daily life activities. The selected body locations were on the arm anterior in correspondence of the biceps brachii muscle for the upper part of the body and on the calf in correspondence to the gastrocnemius muscle for the lower part of the body. Again, the performed activities were the sitting to rest, the walking and the jogging and the measured values of the power output were the range of about 10 μW – 60 μW.

As regards the tests about the application field of the biomechanical energy harvesting, two piezoelectric transducers: a soft PZT transducer (P-876.A12) and a PVDF transducer (LDT4-028k), were placed into a tight suit in proximity to the main human body joints: shoulder, elbow, hip, knee and ankle, respectively, in order to harvest the energy generated by common body movements in the form of casual walking, walking down and up-stairs, jogging and running. The values of the power output measured during the five activities were in the range 5 μW – 75 μW using both transducers for each joint. When examining the user wearability of the two transducers, the PVDF technology is more adequate than soft PZT, because the value of its folding parameter is higher: as a result, it is more comfortable for the user and can better adhere to body movements.

Finally, the PVDF transducer was used for testing the piezoelectric technology as sensor to detect the two main phases of the human gait, the stance and swing phases, respectively. The transducer was placed in the backside of the left knee. The proposed preliminary result shows the potential of using the LDT4-028k PVDF piezoelectric element as both a sensor and an energy harvester in human motion monitoring. This may thus be integrated to detect the phases of gait cycle. While the accuracy in detection of gait phases may need to be more deeply investigated, across a variety of different walking styles and velocities, its combination with biomechanical energy harvesting is a new interesting field that many researchers are investigating for a possible future rich market focused on the development of self-sustainable devices for personalized health monitoring.

As regards the commercial market of the smart clothes for harvesting the energy, the following ***Figure 1E*** shows the current technologies available for the shops and a possible futuristic version of them.

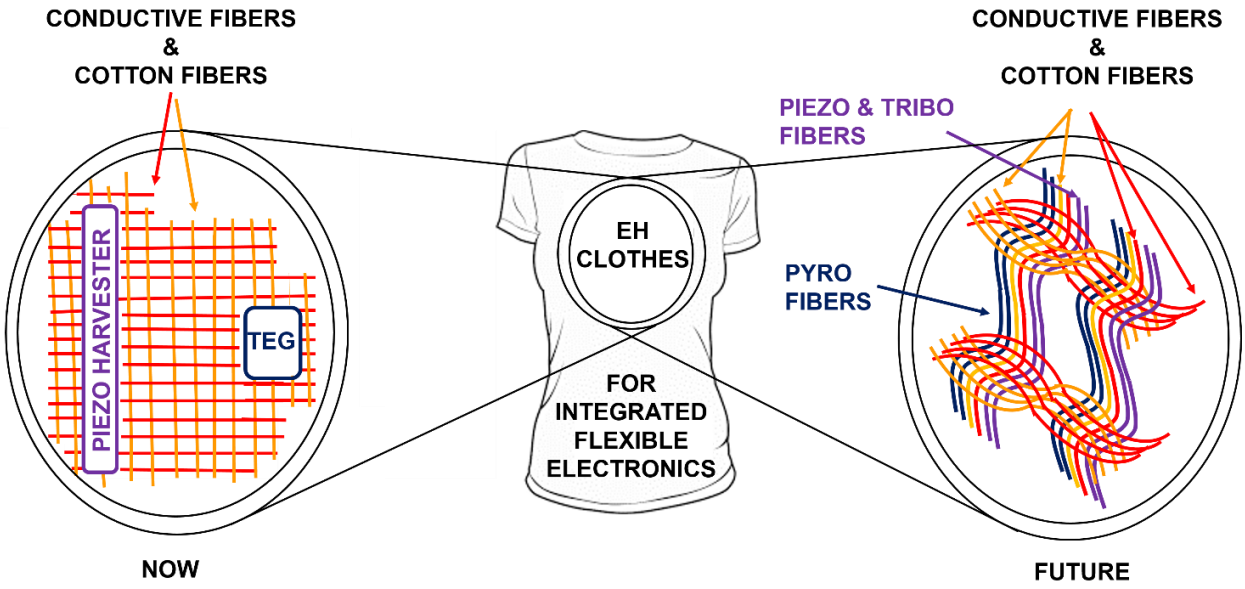

Figure 1E. *The concept for the development of wearable systems that guarantee the monitoring of health and safety of human beings by means the design of smart clothes. These clothes could harvest the energy produced by human body in order to power sensors for the health monitoring. Up to now, (left side), commercial energy harvesters were integrated onto clothes. In the next future (right side), the scientific interest will focus on the development of wearable fabrics made of energy harvester fibers.*

By integrating the textile sensors and the smart fibers within clothes, it will be possible to have smart clothes able to guarantee in a continuous way the health and the safety of human beings.

Finally, it is possible to affirm that the science progress in the fields of nanotechnology, chemistry and electronics is helping the development of such smart technologies, and in the near future, the electronic devices will be more autonomous. For that reason, in the commercial market, a lot of money is going to be invested into new technologies. For the *IDTechEx Research*, over $100 billion will be spent on material for wearable electronics in the next decade; $73 billion will be spent for printed, flexible and organic electronics market in 2025. Over $1 billion will be spent on research on stretchable electronics in 35 years. A $3.7 billion will have been spent for thermal interface materials by 2025, a $5.5 billion market for wearable sensors by 2025 and a $0.8 billion market for piezoelectric energy harvester by 2023. *IDTechEx Research* says again that the e-textile market is entering fast growing phase and will be worth $3 billion within the decade, the market for inorganic

electronics will have risen to $45 billion by 2024. The conductive ink and paste market will grow to over $3 billion in 2025 and the market for batteries and supercapacitors in consumer electronics will be worth $86 billion by 2023.

This study about the new technologies for the field of energy harvesting from the human body may help contribute to the route of the innovation for the monitoring of the vital signals of the people.

LIST OF FIGURES

Figure 1A. *The average power consumed by generic integrated circuit components and sensors, and by implantable devices, in the range of values: 100 nW – 10 mW* 7

Figure 1B. *The energy maintenance in percentage, during the day.*.....10

Figure 2B. *Triboelectric series for some common inorganic and organic materials…* 19

Figure 1C. *A simplified three-layer model of the body tissue, consisting of muscle tissue, fat layer and skin surface*.....28

Figure 2C. *Structure of the TEG module and its equivalent, simplified electrical circuit*.....32

Figure 3C. *Electrical circuit for the measurements of power delivered by the TEG, with the corresponding power track versus the closed circuit voltage.*.....33

Figure 4C. *The TES1-12704 module*.....35

Figure 5C. *A picture of the PVC fabric on the left and the gauze for clothing in the left*.....36

Figure 6C. *The fabrication process of the support fabric band*.....36

Figure 7C. *TEG measurement circuit*.....37

Figure 8C. *The power output generated by the TEG on the arm anterior, in correspondence to the biceps brachii* **(a)** *and the relative temperature difference* **(b)**.....39

Figure 9C. *The power output generated by the TEG on the forearm, in correspondence to the flexor carpi radialis* **(a)** *and the relative temperature difference* **(b)**.....40

Figure 10C. *The power output generated by the TEG on the thigh, in correspondence to the flexor gracilis muscle* **(a)** *and the relative temperature difference* **(b)**.....41

Figure 11C. *The power output generated by the TEG on the calf, in correspondence to the gastrocnemius muscle* **(a)** *and the relative temperature difference* **(b)**.....42

Figure 12C. *The mean values of the power output generated by the TEG on the calf, in correspondence to the gastrocnemius muscle* **(red bars)** *and on the arm anterior in correspondence to the biceps brachii muscle* **(green bars)**.....43

Figure 13C. *The sums of the mean values of the powers generated by the biceps brachii and the gastrocnemius muscles, by performing 10 minutes of physical activity*.....45

Figure 1D. *The rigid-body model for representing the main joints and segments of the human body*……48

Figure 2D. *Picture for representing the human gait cycle*……..49

Figure 3D. *Patterns of joint, muscle and total powers of the shank* **(a)***, foot* **(b)** *and thigh* **(c)**……50

Figure 4D. *Numerical classification of axes of the thin film piezoelectric transducer: 1-length direction, 2-width direction and 3-thickness direction*……53

Figure 5D. *Circuit symbol of the piezoelectric transducer and its electrical measurements circuit*……54

Figure 6D. *The P-876.A12 transducer and the LDT4-028k transducer*……55

Figure 7D. *The blue suit with the green pockets and a green belt*……57

Figure 8D. *Sample of the voltage output measured by using the LDT4-028k transducer placed on the elbow joint for the movement of flexion-extension*……61

Figure 9D. *The calculated mean values of the power output for each value of the load resistor. Error bars represent standard deviations*. **(a)** *P-876.A12*; **(b)** *LDT4-028k*……62

Figure 10D. *Comparison of the calculated grand mean values of power output on each joint for each activity. Error bars represent standard deviations.* **(a)** *P-876.A12;* **(b)** *LDT4-028k*……65

Figure 11D. *The sums of the mean values of the calculated power output on each joint for the activity performed. Error bars represent the standard deviation*……67

Figure 12D. *Position of the LDT4-028k transducer and the Shimmer3 IMU. Location at the back of the knee left leg*……70

Figure 13D. *Comparison between the transducer (LDT4-028k) and gyroscope (Shimmer3 IMU) walking output signals for six different gait speeds*……71

Figure 14D**.** *Detail of one comparison between the transducer (LDT4-028k) and the gyroscope (Shimmer3 IMU) walking output signals (see* ***Figure 13D*** *panel d)*……72

Figure 1E**.** *The concept for the development of wearable systems that guarantee the monitoring of health and safety of human beings by means the design of smart clothes*……..78

LIST OF TABLES

Table 1A. *Characteristics of different energy sources available in the environment, and the corresponding harvested power*.....6

Table 1C. *Skin temperature for different body locations* 30

Table 2C. *Properties of the TES1-12704 module*.... 34

Table 3C. *Results of the sum of the power mean values measured on the skin areas related to biceps brachii and the gastrocnemius muscles*.....45

Table 1D. *Properties of the P-876.A12 and the LDT4-028k transducers*.....55

Table 2D. *Body joints, body joints movements, range of motion and frequency of tests*.....56

Table 3D. *Summary of the common activities and their frequencies*.....57

Table 4D. *Positions of the transducers on the suit and on the belt*.....58

Table 5D. *The chosen fixed values of the resistors*.....60

Table 6D. *The fixed values of the resistors for each joint*.....63

Table 7D. *Comparison between the two transducers based on the five locomotion activities. PZT, lead zirconate titanate*.....66

Table 8D. *Results of the sum of the power grand mean values measured at all of the joints for each activity*...68

Table 9D. *Results shown in* ***Table 8D*** *divided by joint position: upper body and lower body*.....68

REFERENCES

1. Engin, M. et al. (2005) Recent developments and trends in biomedical sensors. Measurement 37 (2), 173-188.

2. Tang, S.L.P. (2007) Recent developments in flexible wearable electronics for monitoring applications. Transactions of the Institute of Measurement and Control 29 (3-4), 283-300.

3. Abd Kadir, E. et al., Indoor WiFi Energy Harvester with Multiple Antenna for Low-power Wireless Applications, IEEE 23rd International Symposium on Industrial Electronics (ISIE), Istambul, TURKEY, 2014, pp. 526-530.

4. Chan, M. et al. (2012) Smart wearable systems: Current status and future challenges. Artificial Intelligence in Medicine 56 (3), 137-156.

5. Patel, S. et al. (2012) A review of wearable sensors and systems with application in rehabilitation. Journal of Neuroengineering and Rehabilitation 9.

6. Milenkovic, A. et al. (2006) Wireless sensor networks for personal health monitoring: Issues and an implementation. Computer Communications 29 (13-14), 2521-2533.

7. Hanson, M.A. et al. (2009) BODY AREA SENSOR NETWORKS: CHALLENGES AND OPPORTUNITIES. Computer 42 (1), 58-65.

8. Lewy, H. (2015) Wearable technologies - future challenges for implementation in healthcare services. Healthcare technology letters 2 (1), 2-5.

9. Kang, H.G. et al. (2010) In Situ Monitoring of Health in Older Adults: Technologies and Issues. Journal of the American Geriatrics Society 58 (8), 1579-1586.

10. Wundersitz, D.W.T. et al. (2015) Classification of team sport activities using a single wearable tracking device. Journal of biomechanics 48 (15), 3975-81.

11. Fida, B. et al. (2015) Varying behavior of different window sizes on the classification of static and dynamic physical activities from a single accelerometer. Medical Engineering & Physics 37 (7), 705-711.

12. Sung-Gu, J. (2015) Wearable Device in Security. International Journal of Security and Its Applications 9 (6), 243-250.

13. Poon, C.C.Y. et al. (2015) Body Sensor Networks: In the Era of Big Data and Beyond. IEEE reviews in biomedical engineering 8, 4-16.

14. He, Y.F. et al. (2011) Optimal Resource Allocation for Pervasive Health Monitoring Systems with Body Sensor Networks. Ieee Transactions on Mobile Computing 10 (11), 1558-1575.

15. Bachmann, C. et al. (2012) Low-Power Wireless Sensor Nodes for Ubiquitous Long-Term Biomedical Signal Monitoring. Ieee Communications Magazine 50 (1), 20-27.

16. Vullers, R.J.M. et al. (2009) Micropower energy harvesting. Solid-State Electronics 53 (7), 684-693.

17. Campagnolo, R. and Kroiss, D. (2012) Toward energy autonomous medical implants. In Energy autonomous micro and nano systems. Edited by Belleville, M. and Condemine, C. John Wiley & Sons, Inc.

18. Hannan, M.A. et al. (2014) Energy harvesting for the implantable biomedical devices: issues and challenges. Biomedical Engineering Online 13.

19. Sodano, H.A. et al. (2005) Comparison of piezoelectric energy harvesting devices for recharging batteries. Journal of Intelligent Material Systems and Structures 16 (10), 799-807.

20. Starner, T. (1996) Human-powered wearable computing. Ibm Systems Journal 35 (3-4), 618-629.

21. Kelly, G. (2006) Body temperature variability (Part 1): A review of the history of body temperature and its variability due to site selection, biological rhythms, fitness, and aging. Alternative Medicine Review 11 (4), 278-293.

22. Ravussin, E. et al. (1986) Determinants of 24-hour energy-expenditure in man - methods and results using a respiratory chamber. Journal of Clinical Investigation 78 (6), 1568-1578.

23. Bouten, C.V.C. et al. (1997) A triaxial accelerometer and portable data processing unit for the assessment of daily physical activity. Ieee Transactions on Biomedical Engineering 44 (3), 136-147.

24. Mitcheson, P.D. et al. (2008) Energy harvesting from human and machine motion for wireless electronic devices. Proceedings of the Ieee 96 (9), 1457-1486.

25. Roundy, S. (2005) On the effectiveness of vibration-based energy harvesting. Journal of Intelligent Material Systems and Structures 16 (10), 809-823.

26. Wang, L. and Yuan, F.G. (2008) Vibration energy harvesting by magnetostrictive material. Smart Materials and Structures 17 (4).

27. Calio, R. et al. (2014) Piezoelectric Energy Harvesting Solutions. Sensors 14 (3), 4755-4790.

28. Koka, A. et al. (2014) Vertically aligned BaTiO3 nanowire arrays for energy harvesting. Energy & Environmental Science 7 (1), 288-296.

29. Kranz, B. et al. (2013) Numerical and experimental characterizations of longitudinally polarized piezoelectric d(15) shear macro-fiber composites. Acta Mechanica 224 (11), 2471-2487.

30. DUrager, C. Energy harvesting for wireless sensors by using piezoelectric transducers. In Proceedings of the 6th EuropeanWorkshop on Structural Health Monitoring, Dresden, Germany, 3–6 July 2012; Vol. 1.

31. Delnavaz, A. and Voix, J. (2014) Flexible piezoelectric energy harvesting from jaw movements. Smart Materials and Structures 23 (10).

32. Halim, M.A. et al. (2013) Frequency up-converted wide bandwidth piezoelectric energy harvester using mechanical impact. Journal of Applied Physics 114 (4).

33. Bai, S. et al. (2013) Two dimensional woven nanogenerator. Nano Energy 2 (5), 749-753.

34. Sirohi, J. and Chopra, I. (2000) Fundamental understanding of piezoelectric strain sensors. Journal of Intelligent Material Systems and Structures 11 (4), 246-257.

35. Renaud, M. et al. (2005) Scavenging energy from human body: Design of a piezoelectric transducer. Transducers '05, Digest of Technical Papers, Vols 1 and 2, 784-787.

36. Jung, W.-S. et al. (2015) Powerful curved piezoelectric generator for wearable applications. Nano Energy 13, 174-181.

37. Shenck, N.S. and Paradiso, J.A. (2001) Energy scavenging with shoe-mounted piezoelectrics. Ieee Micro 21 (3), 30-42.

38. Feenstra, J. et al. (2008) Energy harvesting through a backpack employing a mechanically amplified piezoelectric stack. Mechanical Systems and Signal Processing 22 (3), 721-734.

39. Shukla, R. and Bell, A.J. (2015) PENDEXE: A novel energy harvesting concept for low frequency human waistline. Sensors and Actuators a-Physical 222, 39-47.

40. Pozzi, M. and Zhu, M. (2011) Plucked piezoelectric bimorphs for knee-joint energy harvesting: modelling and experimental validation. Smart Materials & Structures 20 (5).

41. De Pasquale, G. et al. (2013) Energy harvesting from human motion with piezo fibers for the body monitoring by MEMS sensors. 2013 Symposium on Design, Test, Integration and Packaging of Mems/Moems.

42. Kishi, M., et al. "Micro thermoelectric modules and their application to wristwatches as an energy source." Thermoelectrics, 1999. Eighteenth International Conference on. IEEE, 1999.

43. Leonov, V. et al. (2005) Thermoelectric MEMS generators as a power supply for a body area network. Transducers '05, Digest of Technical Papers, Vols 1 and 2, 291-294.

44. Torfs, T. et al. (2006) Body-heat powered autonomous pulse oximeter. Ieee Sensors, Vols 1-3.

45. Leonov, V., et al. "Wearable self-powered wireless devices with thermoelectric energy scavengers." Integration Issues of Miniaturized Systems-MOMS, MOEMS, ICS and Electronic Components (SSI), 2008 2nd European Conference & Exhibition on. VDE, 2008.

46. Leonov, V. and Vullers, R.J.M. (2009) Wearable electronics self-powered by using human body heat: The state of the art and the perspective. Journal of Renewable and Sustainable Energy 1 (6).

47. Leonov, V. et al. (2009) Thermoelectric and Hybrid Generators in Wearable Devices and Clothes. Sixth International Workshop on Wearable and Implantable Body Sensor Networks, Proceedings, 195-200.

48. Lossec, M. et al. (2013) Sizing optimization of a thermoelectric generator set with heatsink for harvesting human body heat. Energy Conversion and Management 68, 260-265.

49. Lossec, M. et al. (2010) Thermoelectric generator placed on the human body: system modeling and energy conversion improvements. European Physical Journal-Applied Physics 52 (1).

50. Voss, T.J. et al., Feasibility of Energy Harvesting Techniques for Wearable Medical Devices, 36th Annual International Conference of the IEEE-Engineering-in-Medicine-and-Biology-Society (EMBC), Chicago, IL, 2014.

51. Brogan, Q. et al. (2014) Solar and Thermal Energy Harvesting with a Wearable Jacket. 2014 Ieee International Symposium on Circuits and Systems (Iscas), 1412-1415.

52. Carmo, J.P. et al. (2010) Thermoelectric Microconverter for Energy Harvesting Systems. Ieee Transactions on Industrial Electronics 57 (3), 861-867.

53. Wang, Z.L. and Song, J.H. (2006) Piezoelectric nanogenerators based on zinc oxide nanowire arrays. Science 312 (5771), 242-246.

54. Li, M. et al. (2017) Evolutionary trend analysis of nanogenerator research based on a novel perspective of phased bibliographic couplings. Nano Energy 34, 93-102.

55. Yang, R. et al. (2009) Power generation with laterally packaged piezoelectric fine wires. Nature Nanotechnology 4 (1), 34-39.

56. Yang, R. et al. (2009) Converting Biomechanical Energy into Electricity by a Muscle-Movement-Driven Nanogenerator. Nano Letters 9 (3), 1201-1205.

57. Lee, S. et al. (2014) Ultrathin Nanogenerators as Self-Powered/Active Skin Sensors for Tracking Eye Ball Motion. Advanced Functional Materials 24 (8), 1163-1168.

58. Lee, S. et al. (2013) Super-Flexible Nanogenerator for Energy Harvesting from Gentle Wind and as an Active Deformation Sensor. Advanced Functional Materials 23 (19), 2445-2449.

59. Chung, S.Y. et al. (2012) All-Solution-Processed Flexible Thin Film Piezoelectric Nanogenerator. Advanced Materials 24 (45), 6022-+.

60. Pradel, K.C. et al. (2014) Solution-Derived ZnO Homojunction Nanowire Films on Wearable Substrates for Energy Conversion and Self-Powered Gesture Recognition. Nano Letters 14 (12), 6897-6905.

61. Persano, L. et al. (2013) High performance piezoelectric devices based on aligned arrays of nanofibers of poly(vinylidenefluoride-co-trifluoroethylene). Nature Communications 4.

62. Park, S.H. et al. (2016) Flexible and Stretchable Piezoelectric Sensor with Thickness-Tunable Configuration of Electrospun Nanofiber Mat and Elastomeric Substrates. Acs Applied Materials & Interfaces 8 (37), 24773-24781.

63. Shin, S.H. et al. (2014) Hemispherically Aggregated BaTiO3 Nanoparticle Composite Thin Film for High-Performance Flexible Piezoelectric Nanogenerator. Acs Nano 8 (3), 2766-2773.

64. Park, K.-I. et al. (2014) Highly-Effi cient, Flexible Piezoelectric PZT Thin Film Nanogenerator on Plastic Substrates. Advanced Materials 26 (16), 2514-2520.

65. Jeong, C.K. et al. (2014) Self-powered fully-flexible light-emitting system enabled by flexible energy harvester. Energy & Environmental Science 7 (12), 4035-4043.

66. Hwang, G.T. et al. (2016) Self-Powered Wireless Sensor Node Enabled by an Aerosol-Deposited PZT Flexible Energy Harvester. Advanced Energy Materials 6 (13).

67. Jeong, C.K. et al. (2015) A Hyper-Stretchable Elastic-Composite Energy Harvester. Advanced Materials 27 (18), 2866.

68. Yang, W. et al. (2013) Harvesting Energy from the Natural Vibration of Human Walking. Acs Nano 7 (12), 11317-11324.

69. Bai, P. et al. (2013) Integrated Multi layered Triboelectric Nanogenerator for Harvesting Biomechanical Energy from Human Motions. Acs Nano 7 (4), 3713-3719.

70. Kang, Y. et al. (2015) Folded Elastic Strip-Based Triboelectric Nanogenerator for Harvesting Human Motion Energy for Multiple Applications. Acs Applied Materials & Interfaces 7 (36), 20469-20476.

71. Song, W.X. et al. (2016) Nanopillar Arrayed Triboelectric Nanogenerator as a Self-Powered Sensitive Sensor for a Sleep Monitoring System. Acs Nano 10 (8), 8097-8103.

72. Meng, B. et al. (2013) Self-powered flexible printed circuit board with integrated triboelectric generator. Nano Energy 2 (6), 1101-1106.

73. Zhang, X.S. et al. (2013) Frequency-Multiplication High-Output Triboelectric Nanogenerator for Sustainably Powering Biomedical Microsystems. Nano Letters 13 (3), 1168-1172.

74. Hecht, D.S. et al. (2011) Emerging Transparent Electrodes Based on Thin Films of Carbon Nanotubes, Graphene, and Metallic Nanostructures. Advanced Materials 23 (13), 1482-1513.

75. Yang, P.-K. et al. (2015) A Flexible, Stretchable and Shape-Adaptive Approach for Versatile Energy Conversion and Self-Powered Biomedical Monitoring. Advanced Materials 27 (25), 3817-3824.

76. Hwang, B.-U. et al. (2015) Transparent Stretchable Self-Powered Patchable Sensor Platform with Ultrasensitive Recognition of Human Activities. Acs Nano 9 (9), 8801-8810.

77. Diaz, A.F. and Felix-Navarro, R.M. (2004) A semi-quantitative tribo-electric series for polymeric materials: the influence of chemical structure and properties. Journal of Electrostatics 62 (4), 277-290.

78. Lee, J.H. et al. (2015) Control of Skin Potential by Triboelectrification with Ferroelectric Polymers. Advanced Materials 27 (37), 5553-5558.

79. Yang, Y. et al. (2013) Human Skin Based Triboelectric Nanogenerators for Harvesting Biomechanical Energy and as Self-Powered Active Tactile Sensor System. Acs Nano 7 (10), 9213-9222.

80. Shi, M.Y. et al. (2016) Self-Powered Analogue Smart Skin. Acs Nano 10 (4), 4083-4091.

81. Sun, J.-G. et al. (2017) A leaf-molded transparent triboelectric nanogenerator for smart multifunctional applications. Nano Energy 32, 180-186.

82. Yang, W.Q. et al. (2014) Triboelectrification Based Motion Sensor for Human-Machine Interfacing. Acs Applied Materials & Interfaces 6 (10), 7479-7484.

83. Dhakar, L. et al., Skin Based Flexible Triboelectric Nanogenerators with Motion Sensing Capability, 28th IEEE International Conference on Micro Electro Mechanical Systems (MEMS), Estoril, Portugal, 2015, pp. 106-109.

84. Dhakar, L. et al. (2016) An intelligent skin based self-powered finger motion sensor integrated with triboelectric nanogenerator. Nano Energy 19, 532-540.

85. Lai, Y.C. et al. (2016) Electric Eel-Skin-Inspired Mechanically Durable and Super-Stretchable Nanogenerator for Deformable Power Source and Fully Autonomous Conformable Electronic-Skin Applications. Advanced Materials 28 (45), 10024-10032.

86. Hyland, M. et al. (2016) Wearable thermoelectric generators for human body heat harvesting. Applied Energy 182, 518-524.

87. Jo, S.E. et al. (2012) Flexible thermoelectric generator for human body heat energy harvesting. Electronics Letters 48 (16), 1015-1016.

88. We, J.H. et al. (2014) Hybrid composite of screen-printed inorganic thermoelectric film and organic conducting polymer for flexible thermoelectric power generator. Energy 73, 506-512.

89. Francioso, L. et al. (2015) Experimental assessment of thermoelectric generator package properties: Simulated results validation and real gradient capabilities. Energy 86, 300-310.

90. Francioso, L. et al. (2013) PDMS/Kapton Interface Plasma Treatment Effects on the Polymeric Package for a Wearable Thermoelectric Generator. Acs Applied Materials & Interfaces 5 (14), 6586-6590.

91. Zeng, W. et al. (2013) Highly durable all-fiber nanogenerator for mechanical energy harvesting. Energy & Environmental Science 6 (9), 2631-2638.

92. Jung, J.H. et al. (2011) Lead-Free NaNbO3 Nanowires for a High Output Piezoelectric Nanogenerator. Acs Nano 5 (12), 10041-10046.

93. Soin, N. et al. (2014) Novel "3-D spacer" all fibre piezoelectric textiles for energy harvesting applications. Energy & Environmental Science 7 (5), 1670-1679.

94. Guo, H.Y. et al. (2016) All-in-One Shape-Adaptive Self-Charging Power Package for Wearable Electronics. Acs Nano 10 (11), 10580-10588.

95. Yang, J. et al. (2015) Eardrum-Inspired Active Sensors for Self-Powered Cardiovascular System Characterization and Throat-Attached Anti-Interference Voice Recognition. Advanced Materials 27 (8), p. 1316.

96. Chen, S.W. et al. (2017) An Ultrathin Flexible Single-Electrode Triboelectric-Nanogenerator for Mechanical Energy Harvesting and Instantaneous Force Sensing. Advanced Energy Materials 7 (1).

97. Li, S. et al. (2015) Cloth-Based Power Shirt for Wearable Energy Harvesting and Clothes Ornamentation. Acs Applied Materials & Interfaces 7 (27), 14912-14916.

98. Zhou, T. et al. (2014) Woven Structured Triboelectric Nanogenerator for Wearable Devices. Acs Applied Materials & Interfaces 6 (16), 14695-14701.

99. Chandrasekhar, A. et al. (2016) Human Interactive Triboelectric Nanogenerator as a Self-Powered Smart Seat. Acs Applied Materials & Interfaces 8 (15), 9692-9699.

100. Liu, L.M. et al. (2016) A triboelectric textile templated by a three-dimensionally penetrated fabric. Journal of Materials Chemistry A 4 (16), 6077-6083.

101. Zhao, Z.Z. et al. (2016) Machine-Washable Textile Triboelectric Nanogenerators for Effective Human Respiratory Monitoring through Loom Weaving of Metallic Yarns. Advanced Materials 28 (46), 10267-10274.

102. Lu, Z. et al. (2016) Silk fabric-based wearable thermoelectric generator for energy harvesting from the human body. Applied Energy 164, 57-63.

103. Kim, M.K. et al. (2014) Wearable thermoelectric generator for harvesting human body heat energy. Smart Materials and Structures 23 (10).

104. Siddique, A.M. et al. (2016) Thermal energy harvesting from the human body using flexible thermoelectric generator (FTEG) fabricated by a dispenser printing technique. Energy 115, 1081-1091.

105. Du, Y. et al. (2015) Thermoelectric Fabrics: Toward Power Generating Clothing. Scientific Reports 5.

106. De Rossi, D. et al. (1999) Dressware: wearable hardware. Materials Science & Engineering C-Biomimetic and Supramolecular Systems 7 (1), 31-35.

107. Edmison, J. et al. (2002) Using piezoelectric materials for wearable electronic textiles. Sixth International Symposium on Wearable Computers, Proceedings, 41-48.

108. Lorussi, F. et al. (2004) Wearable, redundant fabric-based sensor arrays for reconstruction of body segment posture. Ieee Sensors Journal 4 (6), 807-818.

109. Scilingo, E.P. et al. (2005) Performance evaluation of sensing fabrics for monitoring physiological and biomechanical variables. Ieee Transactions on Information Technology in Biomedicine 9 (3), 345-352.

110. Cho, G. et al. (2011) Performance Evaluation of Textile-Based Electrodes and Motion Sensors for Smart Clothing. Ieee Sensors Journal 11 (12), 3183-3193.

111. Tesconi, M. et al. (2006) Wearable kinesthetic system for joint knee flexion- extension monitoring in gait analysis. 2006 28th Annual International Conference of the IEEE Engineering in Medicine and Biology Society, Vols 1-15, 1579-1582.

112. O'Quigley, C. et al. (2014) Characteristics of a Piezo-Resistive Fabric Stretch Sensor Glove for Home-Monitoring of Rheumatoid Arthritis. 2014 11th International Conference on Wearable and Implantable Body Sensor Networks Workshops (Bsn Workshops), 23-26.

113. Rai, P. et al. (2014) Nano- Bio- Textile Sensors with Mobile Wireless Platform for Wearable Health Monitoring of Neurological and Cardiovascular Disorders. Journal of the Electrochemical Society 161 (2).

114. Mattmann, C. et al. (2007) Recognizing upper body postures using textile strain sensors. Eleventh IEEE International Symposium on Wearable Computers, Proceedings, 29-36.

115. Coyle, S. et al. (2009) Textile-based wearable sensors for assisting sports performance. Sixth International Workshop on Wearable and Implantable Body Sensor Networks, Proceedings, 307-311.

116. Lee, S.Y. and Kim, K.J., Piezoelectric Thin Polymer Film and Nanofiber Web Based Sensors Applicable to Smart Textiles for Monitoring Vital Signals and Evaluating Energy Expenditure, 6th Textile Bioengineering and Informatics Symposium (TBIS 2013), Xian Polytechn Univ, Xian, PEOPLES R CHINA, 2013, pp. 153-160.

117. Ozdemir, H. and Kilinc, S. (2015) SMART WOVEN FABRICS WITH PORTABLE AND WEARABLE VIBRATING ELECTRONICS. Autex Research Journal 15 (2), 99-103.

118. Hu, J.Y. et al. (2016) ELECTRICAL PROPERTIES OF PPY-COATED CONDUCTIVE FABRICS FOR HUMAN JOINT MOTION MONITORING. Autex Research Journal 16 (1), 7-12.

119. Muthukumar, N. et al. (2016) Analysis of piezoresistive behavior of polyaniline-coated nylon Lycra fabrics for elbow angle measurement. The Journal of The Textile Institute, 1-8.

120. Shyr, T.W. et al. (2014) A Textile-Based Wearable Sensing Device Designed for Monitoring the Flexion Angle of Elbow and Knee Movements. Sensors 14 (3), 4050-4059.

121. Tognetti, A. et al. (2014) New generation of wearable goniometers for motion capture systems. Journal of Neuroengineering and Rehabilitation 11.

122. Menguc, Y. et al. (2014) Wearable soft sensing suit for human gait measurement. International Journal of Robotics Research 33 (14), 1748-1764.

123. Kramer, R.K. et al., Soft Curvature Sensors for Joint Angle Proprioception, IEEE/RSJ International Conference on Intelligent Robots and Systems, San Francisco, CA, 2011.

124. Yoon, S.G. et al. (2015) Highly Stretchable and Transparent Microfluidic Strain Sensors for Monitoring Human Body Motions. Acs Applied Materials & Interfaces 7 (49), 27562-27570.

125. Yang, Y. and Liu, J. (2013) Evaluation on the Power-Generation Capacity of an Implantable Thermoelectric Generator Driven by Radioisotope Fuel. Journal of Heat Transfer-Transactions of the Asme.

126. Pennes, H.H. (1998) Analysis of tissue and arterial blood temperatures in the resting human forearm (Reprinted from Journal of Applied Physiology, vol 1, pg 93-122, 1948). Journal of Applied Physiology 85 (1).

127. Deng, Z.S. and Liu, J. (2004) Mathematical modeling of temperature mapping over skin surface and its implementation in thermal disease diagnostics. Computers in Biology and Medicine 34 (6), 495-521.

128. Yang, J-H. et al. (2011) A study on skin temperature distribution of the human body as fundamental data for developing heat energy harvesting clothing. Korean Journal of the Science of Emotion and Sensibility 14 (2), 435-444.

129. Zaproudina, N. et al. (2008) Reproducibility of infrared thermography measurements in healthy individuals. Physiological Measurement 29 (4), 515-524.

130. Webb, P. (1992) Temperatures of skin, subcutaneous tissue, muscle and core in resting men in cold, comfortable and hot conditions. European Journal of Applied Physiology and Occupational Physiology 64 (5).

131. Seebeck, J. T. (1826) On the magnetic polarization of metals and minerals by temperature differences. Annals of Physics 82 (3), 253-286.

132. Snyder, G.J. and Toberer, E.S. (2008) Complex thermoelectric materials. Nature Materials 7 (2), 105-114.

133. Zebarjadi, M. et al. (2012) Perspectives on thermoelectrics: from fundamentals to device applications. Energy & Environmental Science 5 (1), 5147-5162.

134. DiSalvo, F.J. (1999) Thermoelectric cooling and power generation. Science 285 (5428), 703-706.

135. Montecucco, A. et al. (2014) The effect of temperature mismatch on thermoelectric generators electrically connected in series and parallel. Applied Energy 123, 47-54.

136. Bandyopadhyay, S. and Chandrakasan, A.P. (2012) Platform Architecture for Solar, Thermal, and Vibration Energy Combining With MPPT and Single Inductor. Ieee Journal of Solid-State Circuits 47 (9).

137. TES1-12704 module. Available online: https://www.gmelectronic.com/m-tes1-12704#product-tabs (accessed on 21 November 2016).

138. Rueterbories, J. et al. (2010) Methods for gait event detection and analysis in ambulatory systems. Medical Engineering & Physics 32 (6), 545-552.

139. Robertson, D.G.E. and Winter, D.A. (1980) Mechanical energy generation, absorption and transfer amongst segments during walking. Journal of Biomechanics 13 (10), 845-854.

140. Umberger, B.R. (2010) Stance and swing phase costs in human walking. Journal of the Royal Society Interface 7 (50), 1329-1340.

141. Merrett, G.V. et al. (2015) Modeling the Effect of Orientation on Human-Powered Inertial Energy Harvesters. Ieee Sensors Journal 15 (1), 434-441.

142. Umberger, B.R. et al. (2013) Generation, absorption, and transfer of mechanical energy during walking in children. Medical Engineering & Physics 35 (5), 644-651.

143. Ottman, G.K. et al. (2002) Adaptive piezoelectric energy harvesting circuit for wireless remote power supply. Ieee Transactions on Power Electronics 17 (5), 669-676.

144. P-876 DuraAct Patch Transducer. Available online: http://www.piceramic.com/product-detail-page/p-876-101790.html (accessed on 21 November 2015).

145. LDT4-028K/Lw/rivets. http://www.te.com/usa-en/plp/ltd-series/Xoyeeo.html (accessed on 21 November 2015).

146. Reese, N.B; Bandy, W.D. Joint Range of Motion and Muscle Length Testing, ninth ed.; W.B. Saunders Company: Philadelphia, PA, USA, 2002; pp. 44–45.

147. LDT1–028K Piezo Sensor with Lead Attachment. Available online: http://www.disensors.com/downloads/products/LDT1-028K%20Application%20Note_898.pdf (accessed on 21 November 2016).

148. Whitepaper: Energy Harvesting Uses the Piezo Effect. Available online: http://www.piceramic.com/applications/piezo-energy-harvesting.html (accessed on 21 November 2016).

149. Aminian, K. et al. (2002) Spatio-temporal parameters of gait measured by an ambulatory system using miniature gyroscopes. Journal of Biomechanics 35 (5), 689-699.

150. Formento, P.C. et al. (2014) Gait Event Detection during Stair Walking Using a Rate Gyroscope. Sensors 14 (3), 5470-5485.

151. Shimmer3 Consensys IMU Development Kit. Available online: http://www.shimmersensing.com/shop/shimmer3-development-kit (accessed on 05 December 2016).

KEYWORDS

Piezoelectricity

Thermoelectricity

Nanogenerators

Locomotion activities

…an infinite thank to my family...

…a special thank to my girlfriend and her family...

…a huge thank to all my friends in Rome, Ferrara, Lamezia Terme and everywhere…

…a big thank to the staff of the Roma Tre University and in particular to the people of the Biolab[3] laboratory…and finally a large thank to the VSB University!!!!